Regenerative Therapy 26 (2024) 442–457

Contents lists available at ScienceDirect

Regenerative Therapy

journal homepage: http://www.elsevier.com/locate/reth

Original Article

High efficiency protocol for platelet derived fibrin gel loaded with mesenchymal stromal cells extracellular vesicles

Enrico Ragni [a, *], Paola De Luca [a], Simona Landoni [a], Federico Valli [b], Leonardo Mortati [c], Silvia Palombella [d], Giuseppe Talò [d], Matteo Moretti [d, e, f, g], Laura de Girolamo [a]

[a] IRCCS Istituto Ortopedico Galeazzi, Laboratorio di Biotecnologie Applicate all'Ortopedia, Via Cristina Belgioioso 173, 20157 Milano, Italy
[b] IRCCS Istituto Ortopedico Galeazzi, Chirurgia Articolare Sostitutiva e Chirurgia Ortopedica (C.A.S.C.O.), Via Cristina Belgioioso 173, 20157 Milano, Italy
[c] Istituto Nazionale di Ricerca Metrologica (INRIM), Str. delle Cacce 91, 10135 Torino, Italy
[d] IRCCS Istituto Ortopedico Galeazzi, Cell and Tissue Engineering Laboratory, Via C. Belgioioso 173, 20157, Milano, Italy
[e] Regenerative Medicine Technologies Lab, Laboratories for Translational Research, Ente Ospedaliero Cantonale, via Chiesa 5, 6500 Bellinzona, Switzerland
[f] Service of Orthopaedics and Traumatology, Department of Surgery, Ente Ospedaliero Cantonale, via Tesserete 46, 6900 Lugano, Switzerland
[g] Euler Institute, Faculty of Biomedical Sciences, Università della Svizzera italiana (USI), via Buffi 13, 6900 Lugano, Switzerland

ARTICLE INFO

Article history:
Received 17 May 2024
Received in revised form
11 June 2024
Accepted 27 June 2024

Keywords:
Mesenchymal stromal cells
Extracellular vesicles
Platelet rich plasma
Platelet gel
Cartilage
Osteoarthritis

ABSTRACT

Introduction: Extracellular vesicles from mesenchymal stromal cells (MSC-EVs) are potent stimulators of naïve cartilage and their injection is studied in clinical trials for cartilage lesions, since often cartilage repaired with conventional approaches is incomplete or less performant leading to joint degeneration. The main pitfall of these innovative approaches is the high EVs dispersion into the joint cavity and consequent low concentration at lesion site. Thus, biological scaffolds for concentration of EVs where needed might be a promising option. This work aimed at producing an enhanced platelet-derived fibrin gel loaded with adipose-derived MSCs (ASCs)-EVs.

Methods: EVs' embedment efficiency in platelet gel, their release and incorporation in OA chondrocytes and cartilage explants were monitored by flow cytometry, microfluidic approaches, scansion electron microscopy and real-time quantitative multimodal nonlinear optics imaging. The effect of released EVs was tested in OA chondrocytes by gene expression studies.

Results: A protocol ensuring high incorporation EVs efficiency in platelet gels was defined, relying on a one-step modification of the standard procedure used in current clinical practice. Trapped EVs were released continuously for up to 4 weeks and uptaken in pathologic chondrocytes and cartilage explants. The release of the EVs-loaded platelet gel had stronger and synergic anti-inflammatory/matrix remodelling effects with respect to both EVs per se and unloaded gel released products.

Conclusions: These results suggest the feasibility of producing a platelet gel loaded with MSC-EVs at high efficiency that can be used as an enhanced tool to foster chondrocyte homeostasis, a key requisite for proper cartilage healing.

1. Introduction

Cartilage, once injured, ends in chondropenia, decreased proteoglycan production and damage to collagen meshwork, causing joint pain, functional impairment and eventually in osteoarthritis (OA) [1]. Cartilage lesions are frequent, with several studies reporting an incidence between 30 and 60% in the general population [2,3] and up to 36% in athletes [4]. In patients with mild symptoms, non-operative treatments are preferred, such as anti-inflammatory drugs, intra-articular hyaluronic acid or steroid injections [5]. In the last years, also orthobiologics have gained

* Corresponding author.
E-mail addresses: enrico.ragni@grupposandonato.it (E. Ragni), deluca.paola@grupposandonato.it (P. De Luca), simona.landoni@grupposandonato.it (S. Landoni), mail@federicovalli.it (F. Valli), l.mortati@inrim.it (L. Mortati), silvia.palombella@grupposandonato.it (S. Palombella), giuseppe.talo@grupposandonato.it (G. Talò), matteo.moretti@grupposandonato.it (M. Moretti), laura.degirolamo@grupposandonato.it (L. de Girolamo).

Peer review under responsibility of the Japanese Society for Regenerative Medicine.

https://doi.org/10.1016/j.reth.2024.06.020

popularity, including injection of blood-derived products, such as platelet rich plasma (PRP) able to reduce the inflammation, improve angiogenesis and promote proliferation of chondrocytes [6]. When self-healing mechanisms, even if stimulated, are not sufficient to fill the gap, surgical interventions are required [7]. Among these, the arthroscopic debridement and subchondral bone marrow stimulation is the most common first-line option for small lesions [8]. The most significant drawback is that the repair tissue is mostly made of fibrocartilage, causing less satisfactory long-term results [9]. Among the research efforts to improve tissue quality and durability of the functional outcome offered by microfractures, PRP showed improved short-term clinical outcomes [10], especially in its formulation as fibrin gel (referred to PRP- or platelet-gel) placed at the site of lesion [11], possibly due to a prolonged release of factors over time [12,13] of the solid form that may last up to three weeks [14]. Nevertheless, the repair tissue remains weaker and far from the native cartilage [11], leading over time to prosthetic intervention.

In the frame of identifying additional factors able to promote healthy cartilage regeneration, extracellular vesicles (EVs) released by mesenchymal stromal cells (MSCs) were recently described. MSC-EVs are enriched in several molecules, including miRNAs, with anti-inflammatory and cartilage regenerative properties [15–17]. Also, MSC-EVs are able to deeply penetrate cartilage thus releasing their cargo [18,19] and enhancing tissue regeneration [20]. Consistently, in several *in vivo* studies, MSC-EVs reduced cartilage damage, improved collagen immunostaining and greater expression of chondrogenic genes and caused macrophage M2 phenotype polarization that promotes resolution of inflammation and cartilage repair [21]. Importantly, the newly formed tissue was almost native hyaline cartilage [22]. Under these premises, recently two clinical trials were registered for the use of injected MSC-EVs for OA (NCT05060107 [23] and NCT05261360 [24]). The main pitfall is that EVs, after injection, are dispersed in the joint cavity with reduced concentration at the site of lesion. Moreover, EVs are cleared in few days suggesting that to maintain the therapeutic efficacy over time several administrations are required.

The aim of this work was to define a protocol to load adipose MSCs (ASCs)-EVs in a platelet gel to ensure their high concentration and constant release where needed, with a focus on chondrocytes. EVs incorporation efficiency and release rate over time was recorded. Eventually, the ability of released particles to be incorporated by human pathological cartilage and chondrocytes and their ability to reduce OA markers in patients' chondrocytes were assessed.

2. Materials and methods

2.1. Adipose tissue collection, ASCs isolation and expansion

Adipose waste material from the abdomen of five healthy female donors (31 ± 5 years old) undergoing aesthetic procedures was processed as previously reported [19]. After 30 min digestion at 37 °C with type I collagenase (Worthington Biochemical Co., Lakewood, NJ, USA), tissues were filtered with a 100 μM strainer, centrifuged at 1000×*g* for 5 min at room temperature and pellets suspended in αMEM + 10% FBS before seeding at 5×10^3 cells/cm^2 at 37 °C (5% CO_2, 95% humidity). Adipose MSCs (ASCs) were selected by plastic adherence and used at passage 1 for analyses.

2.2. Cartilage collection, chondrocytes isolation and expansion

Cartilage was obtained as waste material from 11 osteoarthritis (OA) (Kellgren Lawrence III–IV grade) patients (69 ± 11 years old, six males and five females) undergoing total knee arthroplasty. When chondrocytes were needed, cartilage was digested with 0.15% w/v type II collagenase (Worthington Biochemical, Lakewood, NJ, USA) at 37 °C for 22 h. Then, chondrocytes were isolated for plastic adherence and cultured in DMEM/F12 + 10% FBS and used at passage 1/2. OA phenotype in patients chondrocytes was triggered adding 1 ng/ml Interleukin 1β.

2.3. PRP collection

Fifty-eight PRP samples obtained with the Endoret® system (BTI, Vitoria, Álava, Spain) were collected from patients (mean age 53 ± 11 years, thirty-one males and twenty-seven females) undergoing PRP-based regenerative orthopedic procedures at RE.GA.IN.® Center of IRCCS Ospedale Galeazzi – Sant'Ambrogio. Patients' blood and PRP cell content was assessed with a Sysmex XN-2000 hemocytometer (Sysmex, Kobe, Japan).

2.4. ASCs characterization by flow cytometry

ASCs at passage 1 were analyzed by flow cytometry with a CytoFLEX flow cytometer (Beckman Coulter, Fullerton, CA, USA), collecting at least 30,000 events. Cells were stained for 30 min at 4 °C with the following antibodies: anti-CD90-FITC (REA897, Miltenyi Biotec, Bergisch Gladbach, Germany), CD73-PE (REA804, Miltenyi), CD105-PerCP-Cy5.5 (43A3, BioLegend, San Diego, CA, USA) and CD45-PE-Vio770 (REA747, Miltenyi) and analyzed after one wash with FACS-buffer.

2.5. ASCs secretome production and EVs isolation

ASCs at 90% confluence were washed three times with PBS and fresh αMEM (12 mL per T175 cell culture flask) without FBS was added. After 48 h, secretome was collected and centrifuged at 1000×*g*, 2000×*g* and twice at 4000×*g* (4 °C and 15 min each) to remove broken cells and debris. Secretomes were stored at −80 °C until further use. After secretome removal, ASCs were counted and viability was assessed with a NucleoCounter NC-3000 (Chemometec, Allerod, Denmark).

Before EVs isolation, secretomes were pooled and the pool centrifuged at 100,000×*g* for 3 h at 4 °C in a 70Ti rotor (Beckman Coulter, Fullerton, CA, USA). EV pellets were washed with PBS and suspended in PBS or DMEM/F12 without serum. After count with a NanoSight NS300 system (NanoSight Ltd., Amesbury, UK), EVs concentration was adjusted to 10×10^{10} particles per ml and 10×10^9 EVs' aliquots frozen at −80° until use.

2.6. EVs characterization

Flow cytometry: cleared secretomes were 1:6 diluted while purified EVs were 1:334 diluted with PBS and divided into 3 aliquots: (i) unstained, (ii) 5(6)-carboxyfluorescein-diacetate-succinimidyl-ester (CFDA-SE, Sigma–Aldrich, St. Louis, MO, USA)-stained (1 μM final concentration, 30 min at 37 °C), (iii) after CFDA-SE supplementation and incorporation leading to FITC-fluorescent carboxyfluorescein succinimidyl ester (CFSE), CD9-APC clone HI9A, CD63-APC clone H5C6, CD81-APC clone 5A6, CD73-APC clone AD2 and CD90-APC clone 5E10 (Biolegend, San Diego, CA, USA) stained (30 min at 4 °C). After a further 1:10 dilution with PBS, samples were analyzed with a CytoFlex flow cytometer. At least 30,000 events were collected. FITC-fluorescent nanobeads of 100, 160, 200, 240, 300, 500 and 900 nm (Biocytex, Marseille, France) were used as internal control.

Nanoparticle tracking analysis (NTA): cleared secretomes were 1:3 diluted while purified EVs were 1:167 diluted in PBS and visualized by Nanosight NS-300 system (NanoSight Ltd., Amesbury, UK) (5 recordings of 60 s). NTA software v3.4 provided both

concentration measurements and high-resolution particle size distribution profiles.

2.7. EVs multiplex ELISA assay

The Quantibody® Human Cytokine Array 4000 Kit (RayBiotech, Peachtree Corners, GA, USA) was used to detect two-hundred soluble receptors, chemokines, cytokines, growth and inflammatory factors in purified pooled EVs according to the manufacturers' protocol. A 1:1 dilution was performed and for each analyte and the mean of 4 technical replicates is reported. The amount of each factor in pg/mL was converted into pg/x 10^9 EVs by dividing the concentration value per ml with the number of EVs expressed in x 10^9 per ml in the particle suspension used for the assay.

2.8. Protein–protein interaction networks

Interactome maps of ELISA-identified proteins were generated with the online tool STRING [25] with the following properties: (i) organism, *Homo sapiens*; (ii) meaning of network edges, evidence; (iii) active interaction sources, experiments and databases; (iv) minimum required interaction scores, medium confidence (0.400).

2.9. EV-miRNA quantification

TRIzol reagent was used to dissolve purified pooled EVs and RNA extracted with the miRNeasy Kit and RNeasy CleanUp Kit (Qiagen, Hilden, Germany), following the manufacturer's instruction. Six pg of a non-human synthetic miRNA (*Arabidopsis thaliana* ath-miR-159a) was added to each sample as a spike-in to monitor the technical variability during the isolation and following reactions for eventual equalization of panels A and B of the OpenArray® platform (Life Technologies). Standard reverse transcription and pre-amplification procedures with A and B independent kits were used to generate cDNAs. Real-time RT-PCR analysis with the QuantStudio™ 12 K Flex OpenArray® Platform (QS12KFlex) was then performed as previously described [26]. miRNA expression data from the A and B panels, together covering 754 well-characterized human miRNA sequences from the Sanger miRBase v21, were processed with the Gene Expression Suite Software (Life Technologies). First quartile was identified on Ct values. % of the genetic message was calculated by: i) calculating the ΔCt between the most abundant miRNA and all the others, ii) calculating for all miRNAs the $2^{-\Delta Ct}$ value, iii) calculating the sum of all $2^{-\Delta Ct}$ values, iv) calculating the % for each miRNA following the formula: (Sum $2^{-\Delta Ct}$/Single $2^{-\Delta Ct}$) * 100.

2.10. Preparation of fluorescent EVs

Pooled secretomes were supplemented with 5(6)-carboxyfluorescein-diacetate-succinimidyl-ester (CFDA-SE, Sigma–Aldrich) at a concentration of 10 μM and incubated for 1 h at 37 °C in the dark. For EVs' purification, centrifugation protocol described at point 2.5 was used and 10×10^9 EVs' aliquots frozen at −80° until use.

2.11. Platelet gel preparation and EVs incorporation

Before activation, PRP samples were divided into two 1 ml aliquots and each supplemented either with a suspension of ASC-EVs (10×10^9 EVs per ml of PRP, 100 μl) or the equivalent volume of EVs' suspension solution (100 μl of DMEM/F12 or PBS) without EVs. PRP samples were then activated with 22.8 mM $CaCl_2$, 2 h at 37 °C to form gels. After gelification, the formed fibrin gels and the liquid supernanats above them were separately collected and used immediately or stored at −80 °C for further analyses.

2.12. Scanning electron microscopy of platelet gels

After clotting, supernatnat was removed from platelet gels with or without EVs that were fixed with NaCacodilate 0.1 M pH 7.2, 2.5 % glutaraldheide and 3.7 % formaldheide for 1 h at RT. After fixation, samples were washed with ultra pure distilled water for 30 min, dehydrated with an increasing scale of Ethanol (25, 50, 70, 80, 90, 95, 100%) and placed in a mixture of Ethanol and Hexametyildisilazane (2:1, 1:1, 1:2) for 15 min each and finally transferred in Hexametyldisilazane 100% overnight till complete evaporation. Dry samples were mounted on an alluminium stub, sputtered with platinum (Sputter ACE600, Leica Microsystems, Mannheim, Germany) and observed at a FESEM Sigma (Zeiss, Oberkochen, Germany) operated a 5 KV.

2.13. Visualization of fluorescent EVs incorporation into platelet gel

For standard immunofluorescence analysis, after clotting formation the supernatant was removed and gels with or without EVs were fixed with 3.7 % formaldheide overnight. Afterwards, gels were dehydrated in alchool series and eventually embedded in paraffin and then cut into 4 μm sections for end-point immunofluorescence analysis. Fluorescent images were collected with an IX71 Olympus inverted microscope (Olympus, Tokyo, Japan).

For multimodal microscopy, unprocessed samples were used. The technique allowed to collect images with Coherent Anti-Stokes Raman Scattering (CARS) for fibrin and matrix structures and Two-Photon Excitation Fluorescence (TPEF) for the EVs. The depth of EVs penetration together with the average occupied area and volume were computed using a custom-made ImageJ plugins processing the 3D images as already described [18]. For image acqusition, in the microscopy setup CARS signal was targeted at the CH_2 stretching mode (2848 cm^{-1}), using a Nd:YVO_4 laser emitting 10 ps pulses centered at 1064 nm (Picotrain, HighQLaser, Austria) as the Stokes field and the signal output of an Optical Parametric Oscillator (Levante Emerald OPO) (APE, Berlin, Germany) tuned at about 817 nm with a pulse width of 6 ps as the pump field. The laser repetition rate was 76 MHz. The two beams entered into an upright microscope (BX51WI, Olympus, Tokyo, Japan) through the scanning unit (FluoView FV300, Olympus, Tokyo, Japan). The same OPO signal output at 817 nm was used as excitation source of the TPEF. The total average power at the sample of the excitation pulses was set to about 40 mW. The excitation beams were focused on living samples using a water immersion objective (LUMPLFLN 40XW NA = 0.8, W.D. = 3.3 mm, Olympus) that was cleaned and sterilized with a solution 70% ethanol in water (v/v) before the experiment. A condenser objective (UPLSAPO 10 × objective NA = 0.4, Olympus) was used to collect forward CARS signal at about 663 nm that was optically filtered and then detected using a PMT (R3896, Hamamatsu, Japan). The TPEF signal was acquired in a back-scattering geometry (epi-detection).

2.14. Quantification of EVs incorporation and release

Platelet gels were removed from clotting solution and weight was measured as well as supernatant volumes. For both empty gels and EVs-supplemented gels, a double volume of PBS or DMEM/F12 without serum was added with respect to the wet weight in mg (e.g. 200 μl volume for 100 mg gel weight). After 24 h the supernatant was removed and replaced with the same volume of PBS or DMEM/F12. The same procedure was repeated at 48 h and 1-2-3-4 weeks. Supernatants were analyzed immediately for the

quantification of released EVs by flow cytometry as described as follows or stored at −80 °C for further use.

For EVs incorporation and release quantification, an aliquot of PRP before clotting without and with CFSE-labelled EVs, and aliquots of platelet gel supernatant after clotting and platelet gel supernatants after PBS or DMEM/F12 supplementation were analyzed with CytoFlex flow cytometer. The same acquisition protocol used for EVs immunophenotype characterization was used as previously described. Samples were diluted in PBS to allow a total events/sec number below 2000 with a flow rate of 10 μl/s. Fluorescent EVs were identified as events falling in the FITC channel-gate obtained using PRP without EVs as signal background. To convert events with EVs number the following equation was used: events/sec in the FITC gate * sec/μl * dilution factor * sample volume (μl) = events in the total volume. This number was compared between samples to obtain the percentage of released EV with respect to input EVs (before clotting formation). The number of gel-released EVs in each sample for each time point was then calculated considering EVs added to PRP before clotting as 10×10^9.

2.15. Platelet gel released EVs incorporation into OA chondrocytes in 2D model

Chondrocytes at passage 1 from OA patients were seedeed at a density of 10,000 cells per cm^2. After 24 h, 4 conditions were set: i) control with 1 ng/ml Interleukin 1β to maintain OA phenotype and this pro-inflammatory condition with, ii) purified fluorescent EVs (25,000 particles per cell), iii) 48 h supernatant of platelet gels with released fluorescent EVs (25,000 particles per cell), iv) 48 h supernatant of gels from the same patients without EVs. The equivalent number of EVs in the different conditions was measured by flow cytometry counting FITC-positive events per volume. All conditions were supplemented with 10% ultracentrifuged (100,000×*g*, 9 h, 4 °C) FBS to remove endogenous EVs. After 48 h, chondrocytes were analysed by flow cytometry with a CytoFlex instrument (Beckman) to detect fluorescence in the FITC channel given by incorporated CFSE-labeled EVs. At least 30,000 events were acquired. Mean fluorescence intensity (MFI) of the whole populations was recorded.

2.16. Platelet gel released EVs incorporation into OA chondrocytes in microfluidic model

Under the same experimental conditions previously described, chondrocytes from OA patients were cultured in a microfluidic chip as previously described [19]. Briefly, before seeding in the microfluidic device, OA chondrocytes were stained with CellTracker™ Deep Red Dye (Invitrogen, Eugene, Oregon, USA) and suspended at 3×10^6 cells/ml in human thrombin (4 UI/mL diluted in 40 mM $CaCl_2$, Tisseel kit, Baxter, Stephenville, Texas, USA). This blend was further mixed 1:1 with human fibrinogen (20 mg/mL diluted in PBS, Sigma–Aldrich, St. Louis, Missouri, USA), and injected in the microfluidic compartments. The chips were incubated at RT for 7 min to let the gels polymerize with chondrocytes eventually embedded in the 3D fibrin matrix. Purified or platelet gel released EVs were injected in the central channel and after 48 h chips were fixed with 2% paraformaldehyde for 15 min at RT. Chips not injected with EVs were also fixed and used to define background fluorescence signals. Pictures were taken by a confocal microscope (Leica SP8) acquiring a z-stack of 150 μM corresponding to the entire channel height. Each sliced picture was taken at a distance of 1 μM. To evaluate the interaction between cells and EVs, image analysis was performed by ImageJ software. The macro script developed for a previous work with the same microfluidic devices to automatize the analysis process using as input two-channel z-stack images acquired by confocal microscopy was used [19].

2.17. EVs release from platelet gel and incorporation into OA cartilage

Cartilage waste material from OA patients was cut into pieces of 0.5 cm × 0.5 cm size, with a depth of approximately 0.5–1 mm and placed in 12-well plate. Platelet gel without or with fluorescent EVs were cut into pieces of approximately 0.5 cm length and placed on top of the cartilage fragments. DMEM/F12 medium supplemented with 10 % FBS was added to each well to cover the cartilage/fibrin sandwich with a thin film of liquid, being careful not to allow the gels flush away and therefore float over the cartilage. Cartilage-gel adhesion was further favoured by natural adhesiveness of fibrin. Platelet gels were incubated with cartilage for 48 h before examination under the microscope as previously described for CARS (here for cartilage matrix detection) and TPEF (EVs) signals.

2.18. Activity of EVs-Loaded platelet gel released on OA patients chondrocytes

Under the same experimental conditions previously described, chondrocytes from OA patients at passage 1 were seedeed with a density of 30,000 cells per cm^2 and, after 24 h, treatments were started. When EVs were added, either ultracentrifuge purified or included in the 48 h platelet gel released supernatants, 20,000 particles per cell were administered. The equivalent number of EVs in the administered treatments was measured by flow cytometry counting FITC-positive events per volume. All conditions were supplemented with 10% ultracentrifuged (100,000×*g*, 9 h, 4 °C) FBS to remove endogenous EVs. After 48 h, chondrocytes were dissolved and RNA extracted with the miRNeasy Kit (Qiagen, Hilden, Germany), following the manufacturer's instruction. First-strand cDNAs were synthesized using the iScript cDNA synthesis kit (Bio-Rad Laboratories, CA, USA) and quantifications performed with iTaq Universal SYBR Green Supermix (Bio-Rad Laboratories) in a CFX Opus 96 Real-Time PCR System (Bio-Rad Laboratories). TBP was used as a reference. Primer sequences will be provided upon request. mRNA expression was determined using the relative quantification $2^{-\Delta\Delta CT}$ and fold change reported.

EVs, platelet gel released (all that is released from gels obtained without ASC-EVs) and EVs-loaded gel released (all that is released from gels obtained with ASC-EVs) effect on cell proliferation was measured with an identical experimental approach, with the difference that OA chondrocytes at passage 1 were seedeed with a density of 10,000 cells per cm^2. Cell proliferation was measured with the cell counting kit-8 (CCK-8) cellular proliferation assay (Sigma–Aldrich, St. Louis, MO, USA). At 48 h, CCK-8 solution was administered for 1 h, followed by absorbance measurement of the cell supernatant at 450 nm using a Victor X3 microplate reader (PerkinElmer Life and Analytical Sciences, Shelton, CT, USA). A calibration curve was also prepared at time 0, associating CCK-8 absorbance readouts with those obtained with pre-determined cell numbers, counted with an automated cell counter (Nucleo-Counter® NC-3000™, ChemoMetec, Allerod, Denmark). Fold change for cells per cm^2 with respect to OA chondrocytes at 48 h is reported.

2.19. Statistical analysis

Statistical analysis was performed using GraphPad Prism Software version 8.0.2 (GraphPad, San Diego, CA, US). Shapiro–Wilk normality test (α of 0.01) was used to test normal data

distribution. For analysis of absolute values, for 2 conditions a two-tailed parametric t-test was performed. When the normality test was not passed, a two-tailed non-parametric Wilcoxon test was done. For more than two conditions, a repeated measures one-way ANOVA test was performed, with Tukey's post-hoc test. When the normality test was not passed, a non parametric Friedman test was executed, with Dunn's post-hoc test. For fold changes and ratios, one-sample t-test was performed with hypothesis set as 1. For all tests, the level of significance was set at p-value $\leq$0.05. Values are reported as mean ± SEM.

3. Results

3.1. ASCs and EVs phenotype characterization

ASCs were positive for mesenchymal markers (CD73, 99 % ± 0; CD90, 96 % ± 2; CD105, 67 % ± 8. Mean ± SEM, n = 5) and negative for haematological CD45 (0 % ± 0) (Fig. 1a).

ASCs released 5319 ± 1078 EVs per cell (n = 5) in 48 h. Considering cell culture surface, 41 × 10^6 ± 5 EVs per cm^2 were released. Cell viability was 97 % ± 1 after starvation. Nanoparticle tracking analysis (NTA) technology calculated for the EVs in the supernatants a mean size of 194 nm ± 6 and a mode size of 131 nm ± 6, with a D50 of 167 nm ± 5 (Fig. 1b). Particles were positive for the EV markers CD63 (92 % ± 1) and CD81 (95 % ± 0), while almost negative for CD9 (9 % ± 1, Fig. 1c). With respect to MSC markers that were scored as highly present in the secreting ASCs, lineage CD73 and CD90 gave a strong positivity confirming ASC-EVs identity (90 % ± 0 and 89 % ± 1, respectively, Fig. 1c).

After pooling the supernatants of the different donors and ultracentrifugation, EVs maintained similar size and immunophenotype (Fig. 1d). Mean size was 189 nm, mode 119 nm and D50 162 nm. Purified particles resulted again barely positive for CD9 (8 %), and strongly positive for EV markers CD63 (95 %) and CD81 (95 %) and MSC markers CD73 (91 %) and CD90 (91 %). These results suggested that pooling and the purification process did not affect EVs features.

3.2. miRNAs associated with EVs

By qRT-PCR assay, 344 miRNAs were found associated with purified EVs (Additional file 1). Eighty-six players fell in the first quartile of expression and covered the 99.9 % of the investigated genetic message. Therefore, for the sake of simplicity, only this subset was further studied (Table 1).

To get insights on the OA and cartilage involvement of the first-quartile players, their experimentally validated mRNA targets [27] were selected for analysis (Additional file 2) and compared to OA regulators expressed in joint tissues and cells [28] such as chondrocytes, synoviocytes, and different immune cells, including macrophages and T cells (Table 2). Several pathology-related cytokines/chemokines emerged, encompassing the classical "OA factors" interferon gamma (*IFNG*), tumour necrosis factor (*TNF*), interleukin 1 alpha/beta (*IL1A*/B), interleukin 6 (IL6) and interleukin 8 (*IL8*). Of note, *IFNG*, *TNF* and *IL1B* fell among the five most targeted molecules, with *IFNG* being at the top of the list. Also, other pro-inflammatory interleukins (*IL13*/*11*/*15*/*18*) and chemokines (*CCL5*/*8* and *CXCL12*), alongside *TNFSF11*, a member of the *TNF* cytokine

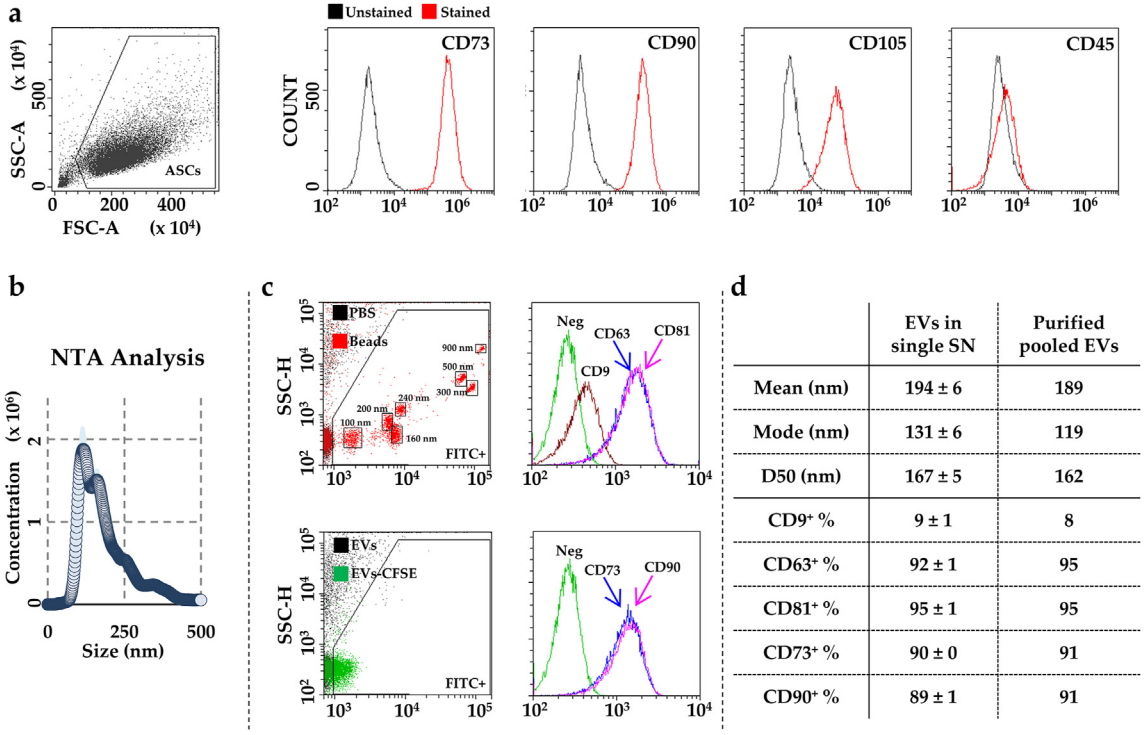

	EVs in single SN	Purified pooled EVs
Mean (nm)	194 ± 6	189
Mode (nm)	131 ± 6	119
D50 (nm)	167 ± 5	162
CD9⁺ %	9 ± 1	8
CD63⁺ %	92 ± 1	95
CD81⁺ %	95 ± 1	95
CD73⁺ %	90 ± 0	91
CD90⁺ %	89 ± 1	91

Fig. 1. Flow cytometry analysis of ASCs and EVs. a) Staining for general mesenchymal (CD73, CD90 and CD105, positive) and haematological (CD45, negative) markers, confirming ASCs identity. Plots of a representative donor are shown. b) EVs size analysis from NTA data of the supernatants of the five donors used in the study. Mean ± SEM are reported. c) Flow cytometer was first calibrated to score FITC-fluorescent particles of nanometric scale (100, 160, 200, 240, 300, 500 and 900 nm). EVs in the supernatants were CFSE stained to allow their identification and gating in the FITC channel. $CFSE^+$ EVs in the $FITC^+$ gate showed positive staining for CD63 and CD81 extracellular vesicle defining molecules, and CD73 and CD90 MSC markers. CD9, another EV postulated marker, gave very low percentage of positive events. Plots of a representative donor are shown. d) Table comparing physical NTA data and immunophenotype profile of both EVs in the supernatants of the five donors used in the study (reported as mean ± SEM) and purified EVs after pooling of the supernatants. Purification process did not affect EVs features.

Table 1
EVs-shuttled miRNAs falling in the first quartile of expression.

miRNA	%	miRNA	%	miRNA	%	miRNA	%
miR-518f-3p	83.351	miR-214-3p	0.059	miR-29a-3p	0.015	miR-483-5p	0.006
miR-636	5.330	miR-574-3p	0.054	miR-17-5p	0.014	miR-148a-3p	0.005
miR-627-5p	2.854	miR-191-5p	0.046	miR-152-3p	0.014	miR-26b-5p	0.005
miR-551b-3p	2.539	miR-199a-3p	0.046	miR-302a-3p	0.014	miR-335-5p	0.005
miR-646	0.933	miR-34a-5p	0.042	miR-127-3p	0.012	let-7a-5p	0.005
miR-1183	0.653	let-7b-5p	0.036	miR-193a-5p	0.012	miR-28-3p	0.005
miR-520e-3p	0.566	miR-1267	0.035	miR-218-5p	0.012	miR-10a-5p	0.005
miR-24-3p	0.538	miR-92a-3p	0.035	miR-328-3p	0.011	miR-299-5p	0.004
miR-125b-5p	0.323	miR-190b-5p	0.032	miR-143-3p	0.010	miR-376a-3p	0.004
miR-21-5p	0.292	miR-30b-5p	0.029	miR-326	0.009	miR-29c-3p	0.003
miR-145-5p	0.201	miR-484	0.026	miR-130a-3p	0.009	miR-532-5p	0.003
miR-523-3p	0.196	miR-26a-5p	0.026	miR-16-5p	0.008	miR-149-5p	0.003
miR-21-3p	0.188	miR-31-5p	0.026	miR-22-3p	0.008	miR-181a-5p	0.003
miR-193b-3p	0.158	miR-30c-5p	0.025	let-7e-5p	0.008	miR-331-3p	0.003
miR-100-5p	0.146	miR-132-3p	0.025	miR-409-3p	0.008	miR-339-5p	0.003
miR-378-3p	0.132	miR-382-5p	0.023	miR-138-5p	0.007	miR-1275	0.003
miR-222-3p	0.117	miR-210-3p	0.021	miR-27a-3p	0.007	let-7g-5p	0.003
miR-221-3p	0.100	miR-224-5p	0.021	miR-365a-3p	0.007	let-7c-5p	0.003
miR-99a-5p	0.095	miR-99b-5p	0.021	miR-27b-3p	0.006	miR-660-5p	0.003
miR-19b-3p	0.086	miR-197-3p	0.020	miR-106b-5p	0.006	miR-146a-5p	0.003
miR-320a-3p	0.069	miR-106a-5p	0.019	miR-376c-3p	0.006		
miR-618	0.064	miR-20a-5p	0.015	miR-342-3p	0.006		

"%" stands for the weight of each miRNA with respect to the entire detected weight.

family, were target of EV-miRNAs. To reinforce the notion of therapeutic potential for ASC-EVs, several growth factors involved with cartilage damage appeared as targets, with vascular endothelial growth factor A (*VEGFA*) being regulated by 14 miRNAs and thereby having the highest total genetic pressure (1.657 %) among all analysed factors. In this category also transforming growth factor beta 1/2 (*TGFB1/2*), whose high levels may promote hypertrophy of cartilage, and connective tissue growth factor (*CTGF*), hepatocyte growth factor (*HGF*) and fibroblast growth factor 1/2 (*FGF1/2*), all related to cartilage and subchondral bone sufferance, fell. Notably, brain-derived neurotrophic factor (*BDNF*) and nerve growth factor (*NGF*), both involved in joint pain similarly to *VEGFA*, were EV-miRNA targets. Last, a number of cartilage matrix degrading enzymes resulted as validated interactors, encompassing several matrix metalloproteinases (*MMP1/2/3/9/13/14*), a disintegrin and metalloprotease (*ADAM12/17*), a disintegrin and metalloproteinase with thrombospondin motif (*ADAMTS9*), cathepsin K (*CTSK*) and serpine E 1 (*SERPINE1*), and their activators like adenomatous polyposis coli (*APC*), plasminogen activator urokinase (*PLAU*) and plasminogen activator tissue type (*PLAT*). In this context of overall targeting of OA-inducer and cartilage-degradation factors, EV-miRNAs also may target few molecules with protective features, such as the anti-inflammatory *IL4*, the cartilage protective erythropoietin (*EPO*) and insulin like growth factor 1/2 (*IGF1/2*), alongside some tissue inhibitors of MMPs (*TIMP1/2/3*).

Eventually, to get a broader picture of EVs-embedded miRNAs that goes beyond the regulation of single factors, their acknowledged role for cartilage homeostasis [29] and macrophage polarization [30] was studied (Table 3). Regarding cartilage, the majority (16 out of first quartile EV-miRNAs) have a protective function. The most impactful players are miR-24-3p (0.538 %), miR-125b-5p (0.323 %) and miR-193b-3p (0.158 %), with an overall weight for this category of 1.476 %. This value heavily dropped for the 7 identified destructive miRNAs, that stands at 0.388 %, for an almost 4-fold reduction. Also, 3 miRNAs with dual function were identified, for a 0.211 % weight. Concerning macrophages, an equal number of miRNAs (6) characterized the categories pro-M1 (pro-inflammatory) and pro-M2 (anti-inflammatory), albeit the protective players had a 3-fold higher amount (0.739 % vs 0.254 %) mainly due to miR-24-3p. Therefore, as for the targeted single factors, also at a more general level EV-miRNAs have a potential therapeutic feature for both damaged cartilage and inflammation resolution.

3.3. Factors associated with EVs

By ELISA assay, 163 factors were found associated with purified EVs (Additional file 3). Fifteen factors were detected with an amount >1 ng/10^9 EVs (Table 4), with Insulin-like growth factor-binding protein (IGFBP)-4 and IGFBP-3 being the most abundant ones at a concentration >10 ng/10^9 EVs (44 and 20, respectively). In this group of abundant molecules, other two IGFBPs were found, namely 2 and 6. Other highly EVs-associated proteins were, among others, two Bone morphogenetic protein (BMP)-5/7, two Tissue inhibitor of metalloproteinase (TIMP)-1/2, two growth factors like Transforming growth factor beta (TGFb1) and Fibroblast growth factor (FGF-4), and two receptors such as Interleukin 6 receptor (IL-6R) and Tumour necrosis factor receptor 2 (TNF RII). Other 43 factors were detected between 1 and 0.1 ng/10^9 EVs (Table 4) and other 65 between 0.1 and 0.01 ng/10^9 EVs. Eventually, 40 proteins were barely detectable with an abundance <0.01 ng/10^9 EVs.

Being in our protocol 10×10^9 EVs supplemented to 1 ml PRP, those factors present at a concentration >0.1 ng/10^9 EVs, and thus >1 ng in 10×10^9 EVs, were analysed by functional protein association network approach. Two main clusters emerged, encompassing factors with different functions. Notably, all factors of the smaller and tighter cluster and several of the second and loose one were involved in Inflammatory (gene ontology, GO:0006954) and Immune (GO:0006955) response (Fig. 2a and Additional file 4a). Also, several factors were related to Chemotaxis (GO:0006935) (Fig. 2a and Additional file 4b). Connecting these two areas, many of the identified proteins regulates the movement of immune cell types, including cells involved in joint inflammation and degeneration such as Lymphocyte (GO:0048247), Monocyte (GO:0002548) and Neutrophils (GO:0030593) (Additional file 4b). Moreover, some of the factors in the second and loose cluster were involved in Cartilage (GO:0051216) and Connective tissue (GO:0061448) development, as also indicated by their ability to shape the Reactome Pathway Extracellular matrix organization (HSA-1474244) (Fig. 2b and Additional file 4c).

Table 2
OA-related regulators targeted by first quartile EV-miRNAs.

CYTO/CHEMO	ACTIVITY	% WEIGHT	TARGETING miRNAs
IFNG	Pro-inflammatory	0.564	miR-16-5p,24-3p,27a-3p,181a-5p,409-3p
IL4	Anti-inflammatory	0.538	miR-24-3p
TNF	Pro-inflammatory	0.407	miR-16-5p,17-5p,34a-5p,125b-5p,130a-3p,143-3p
EPO	Cartilage regeneration	0.323	miR-125b-5p
IL1B	Pro-inflammatory	0.292	miR-21-5p
CXCL12	Cartilage degradation	0.128	miR-31-5p,146a-5p,221-3p
WNT1	Cartilage development	0.083	let-7a-5p,7e-5p,miR-22-3p,34a-5p,148a-3p,152-3p,
CCL5	Cartilage degradation	0.062	miR-146a-5p,214-3p
EDN1	Cartilage hypertrophy	0.049	let-7a-5p,7b-5p,miR-130a-3p
IL6	Pro-inflammatory	0.047	let-7a-5p,7c-5p,miR-26a-5p,146a-5p,149-5p,365a-3p
IL1A	Pro-inflammatory	0.046	miR-191-5p
CCL8	Pro-inflammatory	0.035	miR-92a-3p
IL11	Pro-inflammatory	0.025	miR-30c-5p
CSF1	Cartilage degradation	0.023	miR-130a-3p,152-3p
IL18	Pro-inflammatory	0.009	miR-130a-3p
TNFSF11	Subchondral bone	0.006	miR-106b-5p
IL15	Cartilage degradation	0.005	miR-148a-3p
SPP1	Cartilage ageing	0.004	miR-299-5p
IL13	Anti-inflammatory	0.003	let-7g-5p
IL8	Pro-inflammatory	0.003	miR-146a-5p
CD40LG	Pro-inflammatory	0.003	miR-146a-5p
GF			
VEGFA	Cartilage degeneration/pain	1.657	miR-16-5p,17-5p,20a-5p,21-5p,29a-3p,29c-3p,34a-5p,106a-5p,106b-5p,145-5p,181a-5p,199a-3p,214-3p,
TGFB1	Cartilage hypertrophy	0.604	miR-24-3p,130a-3p,146a-5p,574-3p
ANGPT2	Related to OA severity	0.524	miR-125b-5p,145-5p
TGFB2	Cartilage hypertrophy	0.499	miR-21-5p,145-5p,148a-3p,
IGF2	Cartilage protection	0.474	let-7a-5p,miR-100-5p,125b-5p
IGF1	Cartilage protection	0.349	let-7e-5p, miR-26a-5p,26b-5p,27a-3p,29a-3p,130a-3p,145-5p,190b-5p,199a-3p,
CTGF	Cartilage degradation	0.268	miR-26a-5p,26b-5p,30c-5p,143-3p,145-5p
FGF10	Inhibits synovial fibrosis	0.201	miR-145-5p
LEP	Pro-inflammatory	0.100	miR-221-3p
HGF	Reduces mineralization	0.086	miR-16-5p,26a-5p,26b-5p,199a-3p,
INHBB	Chondrocyte proliferation	0.042	miR-34a-5p
BDNF	Pain enhancer	0.042	miR-10a-5p,16-5p,22-3p,210-3p
BMP2	Related to OA severity	0.038	let-7a-5p,miR-17-5p,106a-5p,
FGF2	Cartilage degradation	0.022	miR-16-5p,152-3p
FGF1	Cartilage degradation	0.009	miR-326
BMP6	Proteoglycan synthesis	0.008	miR-22-3p
NGF	Pain enhancer	0.005	let-7a-5p
PROTEASES			
MMP14	Cartilage degradation	0.762	miR-10a-5p,22-3p,24-3p,143-3p,145-5p
TIMP3	Cartilage protection	0.711	miR-17-5p,21-3p,21-5p,221-3p,222-3p
MMP13	Cartilage degradation	0.497	miR-27b-3p,100-5p,125b-5p,127-3p,143-3p
MMP2	Cartilage degradation	0.482	miR-17-5p,29a-3p,29c-3p,106b-5p,125b-5p,143-3p,218-5p,221-3p
SERPINE1	Cartilage degradation	0.371	miR-10a-5p,30b-5p,30c-5p,99a-5p,143-3p,145-5p,148a-3p
APC	MMP activator	0.355	miR-27a-3p,106a-5p,106b-5p,125b-5p
MMP9	Cartilage degradation	0.338	let-7e-5p,miR-21-5p, miR-132-3p,143-3p,149-5p
MMP1	Cartilage degradation	0.318	miR-145-5p,222-3p
PLAT	Cartilage degradation	0.292	miR-21-5p
ADAM17	Cartilage degradation	0.241	miR-26a-5p,145-5p,152-3p
PLAU	Cartilage degradation	0.158	miR-193b-3p
TIMP2	Cartilage protection	0.034	miR-20a-5p,106a-5p
MMP3	Cartilage degradation	0.026	miR-31-5p
ADAM12	Cartilage degradation	0.018	miR-29a-3p,29c-3p
ADAMTS9	Cartilage degradation	0.015	miR-29a-3p
TIMP1	Cartilage protection	0.010	miR-138-5p,181a-5p
CTSK	Cartilage degradation	0.003	miR-29c-3p
MMP15	Cartilage degradation	0.003	miR-29c-3p

"GF" stands for Growth Factors; "% weight" for the summary of single miRNAs weight in EVs.

3.4. EVs supplementation affects platelet gel soaking with plasma, weight and ultrastructure

To obtain wet clots (starting from 1 ml PRP) without excessive soaking of residual plasma, platelet gels were let leaking for 10 min until no more dripping liquid was visible. EVs addition led to a significantly higher released volume, being 127 μl ± 13 for control gels and 182 μl ± 14 for gels obtained after EVs addition (n = 21, p-value <0.01). Moreover, resulting wet platelet gels were heavier with EVs, with a weight of 110 mg ± 10 (no EVs) and 239 mg ± 16 (with EVs) (n = 22, p-value <0.0001). The increased weight was due both to an augmented imbibition of liquid (40 μl ± 8 no EVs; 139 μl ± 13 with EVs; n = 22, p-value <0.0001) and to a higher weight of gel matrix (70 mg ± 4 no EVs; 99 mg ± 9 with EVs; n = 22, p-value <0.01).

By scanning electron microscopy (Fig. 3a and b) it was possible to observe that fibrin fibrils were clearly visible in both gels, where gels without EVs showed a more regular structure with bundle of fibres whereas gels with EVs have a more complex organization with a more wrinkled appearance. At higher magnification, fibrins

Table 3
Role of EV-miRNAs at cartilage and macrophage levels.

CARTILAGE		
PROTECTIVE	*%*	*ROLE*
miR-24-3p	0.538	Regulates chondrocyte senescence
miR-125b-5p	0.323	Prevents aggrecan loss
miR-193b-3p	0.158	Regulates inflammation
miR-222-3p	0.117	Controls cartilage degradation
miR-221-3p	0.100	Prevents ECM degradation
miR-320a-3p	0.069	Chondrocyte viability
miR-199a-3p	0.046	Anti-catabolic
miR-92a-3p	0.035	Anti-catabolic
miR-26a-5p	0.026	Cartilage homeostasis
miR-210-3p	0.021	Promotes chondrocyte proliferation
miR-17-5p	0.014	Induces autophagy
miR-130a-3p	0.009	Anti-inflammatory
miR-27b-3p	0.006	Anti-catabolic
miR-148a-3p	0.005	Promotes hyaline cartilage
miR-26b-5p	0.005	Cartilage homeostasis
miR-149-5p	0.003	Anti-inflammatory
Total	**1.476**	
DESTRUCTIVE		
miR-21-5p	0.292	Negatively regulates chondrogenesis
miR-34a-5p	0.042	Apoptosis
miR-30b-5p	0.029	ECM degradation
miR-16-5p	0.008	Cartilage degradation
miR-138-5p	0.007	Cartilage degradation
miR-483-5p	0.006	Stimulates chondrocyte hypertrophy
miR-181a-5p	0.003	Pro-inflammatory
Total	**0.388**	
DUAL		
miR-145-5p	0.201	Chondrocyte proliferation/cartilage degradation
miR-365a-3p	0.007	Prevents ECM loss/pro-inflammatory
miR-146a-5p	0.003	Chondrocyte proliferation/Promotes autophagy
Total	**0.211**	
MACROPHAGES		
PRO M1	*%*	
miR-145-5p	0.201	
miR-27b-3p	0.006	
miR-130a-3p	0.009	
miR-26a-5p	0.026	
miR-26b-5p	0.005	
miR-27a-3p	0.007	
Total	**0.254**	
PRO M2		
miR-24-3p	0.538	
miR-146a-5p	0.003	
miR-181a-5p	0.003	
miR-34a-5p	0.042	
miR-222-3p	0.117	
let-7b-5p	0.036	
Total	**0.739**	

"%" stands for single miRNA weight in EVs.

Table 4
Factors associated with purified EVs at a concentration >0.1 ng/exp9 EV.

FACTOR	ng/exp9 EVs	DESCRIPTION
IGFBP4	44.1792	Insulin-like growth factor-binding protein 4
IGFBP3	19.7445	Insulin-like growth factor-binding protein 3
TGFB1	7.4277	Transforming growth factor beta-1
BMP7	5.7414	Bone morphogenetic protein 7
BMP5	5.0289	Bone morphogenetic protein 5
ICAM1	4.0753	Intercellular adhesion molecule 1
IL6R	2.9192	Interleukin-6 receptor subunit alpha
IGFBP2	2.4930	Insulin-like growth factor-binding protein 2
FGF4	1.4319	Fibroblast growth factor 4
TIMP1	1.3786	Metalloproteinase inhibitor 1
TNFRSF1B	1.1151	Tumour necrosis factor receptor superfamily member 1B
CD14	1.0394	Monocyte differentiation antigen CD14
IGFBP6	1.0216	Insulin-like growth factor-binding protein 6
TIMP2	1.0163	Metalloproteinase inhibitor 2
CCL26	1.0058	C–C motif chemokine 26
MIF	0.9628	Macrophage migration inhibitory factor
PF4	0.8679	Platelet factor 4
CCL5	0.8558	C–C motif chemokine 5
EGFR	0.8515	Epidermal growth factor receptor
IGFBP1	0.6944	Insulin-like growth factor-binding protein 1
CSF1R	0.6386	Macrophage colony-stimulating factor 1 receptor
ICAM2	0.5986	Intercellular adhesion molecule 2
KDR	0.5568	Vascular endothelial growth factor receptor 2
TNFRSF1A	0.5547	Tumour necrosis factor receptor superfamily member 1A
MST1	0.5125	Hepatocyte growth factor-like protein
PDGFB	0.4803	Platelet-derived growth factor subunit B
KIT	0.4466	Mast/stem cell growth factor receptor Kit
BDNF	0.4387	Brain-derived neurotrophic factor
SERPINE1	0.4119	Plasminogen activator inhibitor 1
PECAM1	0.3802	Platelet endothelial cell adhesion molecule
SELL	0.3372	L-selectin
TGFB1	0.2844	Human TGF-beta
PDGFA	0.2409	Platelet-derived growth factor subunit A
CXCL16	0.2316	C-X-C motif chemokine 16
IL5	0.2265	Interleukin-5
PPBP	0.2123	Platelet basic protein
CXCL5	0.2058	C-X-C motif chemokine 5
GDNF	0.1994	Glial cell line-derived neurotrophic factor
SPP1	0.1912	Osteopontin
IL7	0.1890	Interleukin-7
HGF	0.1878	Hepatocyte growth factor
FGF7	0.1823	Fibroblast growth factor 7
NTF3	0.1779	Neurotrophin-3
IL6ST	0.1764	Interleukin-6 receptor subunit beta
VEGFA	0.1693	Vascular endothelial growth factor A
CCL21	0.1682	C–C motif chemokine 21
CCL19	0.1638	C–C motif chemokine 19
PDGFA	0.1584	Platelet-derived growth factor subunit A
FST	0.1552	Follistatin
IFNL1	0.1500	Interferon lambda-1
CCL1	0.1432	C–C motif chemokine 1
TGFB3	0.1357	Transforming growth factor beta-3
ANG	0.1299	Angiogenin
SIGLEC5	0.1247	Sialic acid-binding Ig-like lectin 5
IL31	0.1210	Interleukin-31
CCL24	0.1052	C–C motif chemokine 24
CDH1	0.1042	Cadherin-1
IL18BP	0.1041	Interleukin-18-binding protein

in clots with EVs were more tightly packed with the formation of smaller and more narrow spaces and cavities. Thus, gels formed with EVs result in a spongy structure with tighter fibrils and smaller holes justifying both the increased weight and the increased ability to retain plasma.

3.5. EVs fully embed platelet gel matrix

EVs gave rise to a positive and homogenous fluorescent signal along the whole length of the platelet gel and across its section (Fig. 4). To corroborate this result, gels with EVs were analysed by multimodal microscopy that allows to collect images of fluorescence and matrix without fixation and processing of the samples (Fig. 5). Without EVs, a very low level of autofluorescence was detected (Fig. 5a) whereas, confirming previous findings, EVs homogenously permeated the gels, as clearly emerging from the 3D reconstructions of the samples focusing on their surface (Fig. 5b) or section (Fig. 5c). Moreover, EVs and fibrin signals were completely superimposable until the depth of one hundred microns that was the limit of detection of this technique inside the intact platelet gel. Thus, EVs fully and homogeneously permeate gel structure.

3.6. EVs are efficiently incorporated into platelet gels and released over time

The amount of EVs incorporated into platelet gels was 58 % ± 2 (n = 17) of the input (10×10^9 EVs) added to 1 ml PRP before clot

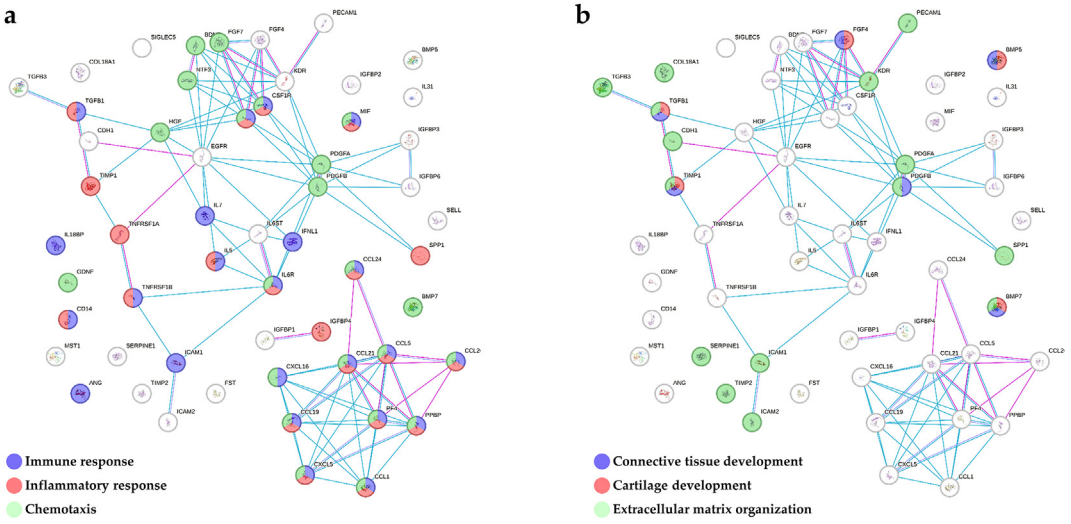

Fig. 2. Functional association network for EVs-associated factors with concentration > 0.1 ng/exp^9 EVs using the online tool STRING. a) Proteins related to inflammatory and motility gene ontology categories are shown. b) Proteins related to cartilage and extracellular matrix are shown. The blue connections are for proteins with known interactions based on curated databases; violet connections for proteins with experimentally determined interactions. Empty nodes, proteins of unknown 3D structure; filled nodes, known or predicted 3D structure.

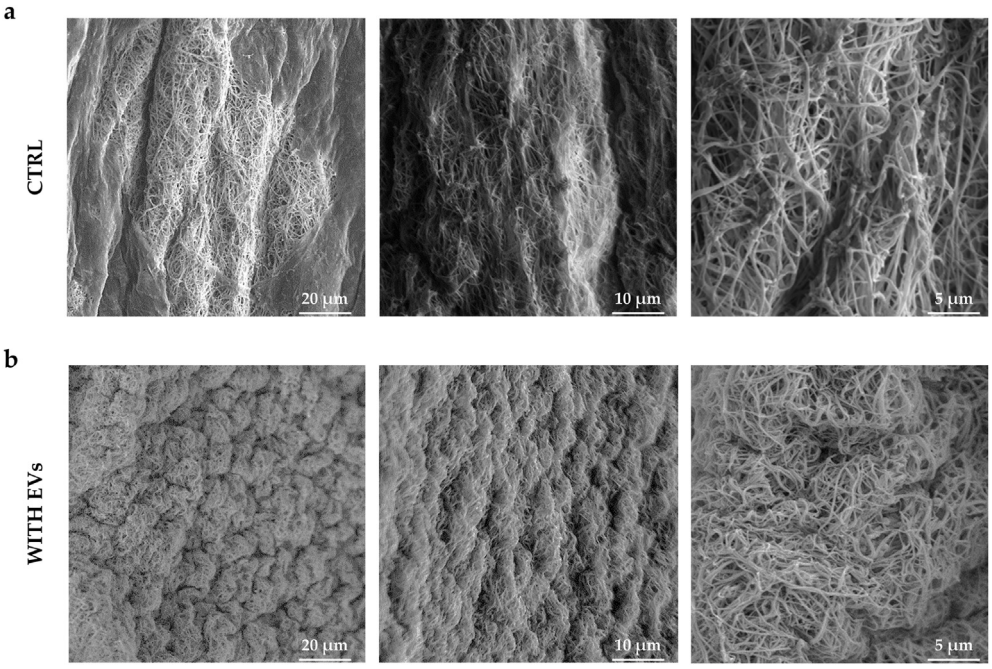

Fig. 3. Scanning electron microscopy analysis of platelet gels without and with EVs. a) Control platelet gel showed presence of fibrin fibrils organized in regular bundles. b) EVs supplementation leads to the formation of a less organized structure with grooves and rolls. Fibrils are more interconnected with smaller empty spaces. Representative pictures are shown.

formation. Taking into account wet gel weight, $54 \times 10^6 \pm 6$ EVs per mg were included. EVs release over time was monitored for a period up to 4 weeks. An important point to describe EVs release kinetics is that two main subgroups could be identified based on gel stability over time. The first one, composed of 10 gels, was characterized by high stability, with clots being solid for the whole time of analysis. The second one, including 7 gels, was composed of clots that started to dissolve spontaneously during the investigation period. In this group, clot stability was extremely variable, with some starting to dissolve after one week and others at 2, 3 or 4 weeks. Concerning the stable gels, amount and kinetics of released EVs per mg of clot are reported in Fig. 6a and b, showing both single time periods and cumulative data. In the first 24 h, 6.10 % ± 0 00.97 (n = 10) of incorporated EVs exited the clots, followed by a 1.01 % ± 0.18 in the second day. In the 3–7 days' period, another 0.32 % ± 0.05 of embedded particles was delivered. In the next 3 weeks, a constant release (0.07 % ± 0.01 for week 2, 0.05 % ± 0.01 for week 3 and 0.07 % ± 0.01 for week 4) was monitored. Overall, during the 4 weeks of the analysis, 7.61 % ± 1.15 of incorporated EVs exited the gels, with 92.35 % ± 1.47 of this amount in the first 48 h. The situation was different and donor-dependent for the other platelet gels with reduced stability (Fig. 7a). For those gels starting to

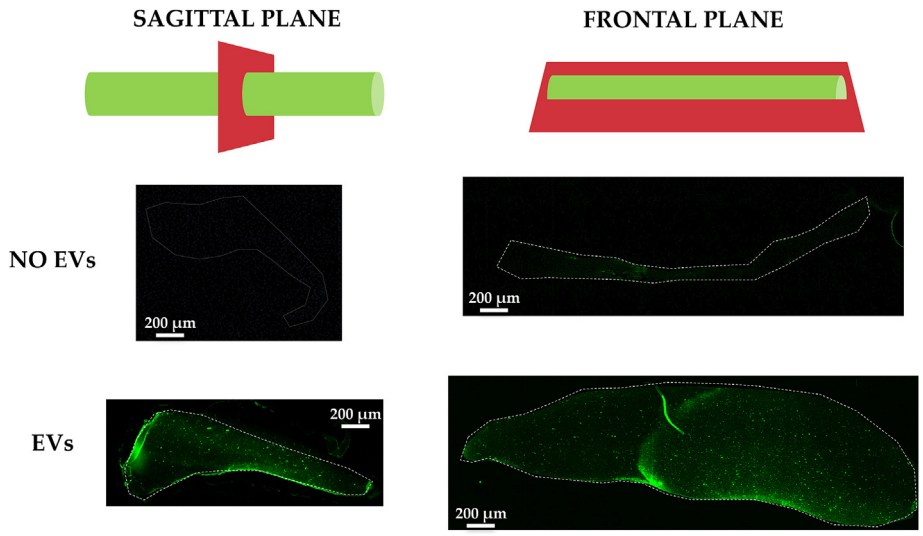

Fig. 4. EVs incorporation in platelet gel visualized by conventional microscopy. Sagittal and frontal plane of a representative platelet gel without and with fluorescent EVs. It is possible to observe a homogenous EVs signal (in green) all over the gel section, including its centre. Representative pictures are shown.

dissolve at 1–3 weeks, a small clot was visible after 28 days. For those ones dissolving at 4 weeks, clot size was similar to stable gels, although starting to be reduced in dimension. Of note, platelet gel dissolution was concomitant with an increase in EVs release (Fig. 7b). Consistently, for gels that started to dissolve at 1–3 weeks, the cumulative EVs release was 25.75 % ± 2.57 (n = 4) of the incorporated particles, while for those initiating to reduce at 4 weeks, the value was 8.67 % ± 1.48 (n = 3).

3.7. Released EVs interacts with chondrocytes and are uptaken by cartilage explant

Since EVs release from both stable and unstable platelet gels at 48 h was comparable, particles collected after 2 days were used to test their conserved ability, with respect to purified EVs, to interact with OA patients' chondrocytes in both 2D and microfluidic 3D models as well as with OA patients' cartilage

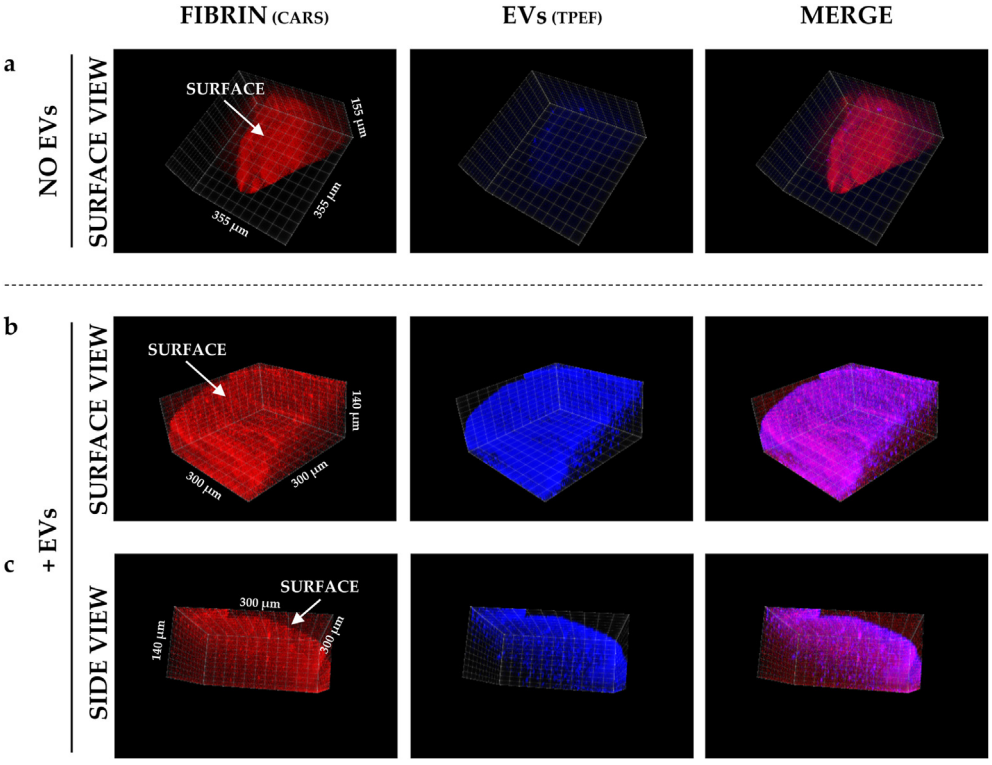

Fig. 5. Three-dimensional reconstructions of the platelet gel without and with fluorescent EVs. CARS signal originating by fibrin is shown in red and the TPEF signal related to the EVs fluorescence is shown in blue, with the two channels merged giving rise to a violet colour in case of co-localization of signals. In the top right corner of each image, close to the boundary box are shown the dimensions in μm starting from the origin vertex. a) View of the surface of platelet gel without EVs showing very low autofluorescence signal in the TPEF (EVs) channel. b) View of the surface of platelet gel with EVs. c) Side view showing homogeneous presence of EVs across gel depth. Representative pictures are shown.

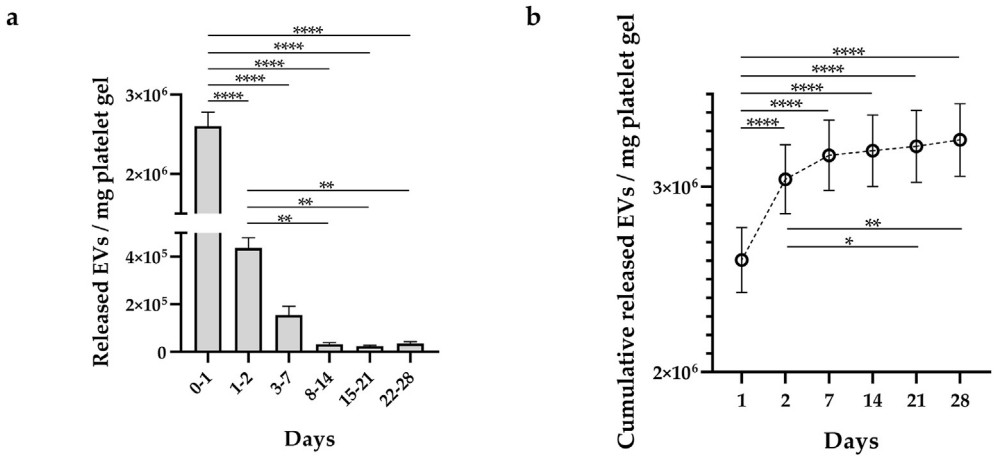

Fig. 6. EVs release over time from stable platelet gels. a) EVs released per mg of wet platelet gel is more pronounced in the first 48 h, followed by a reduced but constant exit between the second and the fourth week. Mean ± SEM, n = 10. ** for p-value <0.01 and **** for p-value <0.0001. Only significant differences are indicated. b) The cumulative EVs release over time is reported with continuous exit in the last 3 weeks leading to significant difference with respect to values at 48 h. Mean ± SEM, n = 10. * for p-value <0.05, ** for p-value <0.01 and **** for p-value <0.0001. Only significant (p-value <0.05) differences are indicated.

explants. Concerning EVs-cell interaction, it resulted similar between purified particles and gel released EVs (Fig. 8a), with no statistical (p-value <0.05) difference in the MFI values in the FITC channel (Fig. 8b). Also, released of platelet gel without EVs did not influence background fluorescence of chondrocytes. To confirm similar interaction properties, the same amount of purified EVs and EVs in platelet gel released were administered to OA patients' chondrocytes grown in a microfluidic model to mimic the 3D environment cells are embedded within in the cartilage (Fig. 8c). Similar to 2D cultures, pictures of 3D cultures confirmed that after 48 h EV fluorescence was clearly associated with OA chondrocytes. The analysis of the intensity of total EV fluorescence confirmed no significant difference in the two conditions (arbitrary MFI of chondrocytes with pure EVs *vs* chondrocytes with released of EVs-loaded platelet gel: 18.2 ± 0.4 *vs* 19.1 ± 2.0, n = 3, p-value of 0.7644) (Fig. 8d), corroborating EVs interaction also when cells are in a 3D environment and suggesting their ability to penetrate ECM matrix. Multimodal microscopy on cartilage explants from OA patients allowed to observe that after 48 h of direct contact with EVs' loaded platelet gels a positive signal up to a depth of >200 μm could be detected (Fig. 9).

3.8. PRP and EVs effect on OA patients' chondrocytes

In a 2D model of OA chondrocytes maintained in pathologic condition, purified EVs were able to significantly (p-value <0.05) reduce the amount of several mRNAs related to cartilage pathology (Fig. 10a, and Additional file 5 for whole data). In particular, the major pro-inflammatory cytokines *IL6* and *IL8* and ECM degrading enzymes *MMP1* and *MMP3* emerged with contraction between 30 and 60 %. *IL1β*, coding for another crucial pro-inflammatory factor, had a tendency (p-value <0.1) towards down-regulation (20 %). Platelet gel released (PGR), mostly composed of PRP factors, had a different impact on chondrocytes. After treatment, *IL1β* and *IL11* resulted highly up-regulated, 25 and 13 fold, respectively, as well as *FGF2* (2.1 fold). On the contrary, among downregulated genes, *IL6*, *CCL5*/8, *TNFSF11* and *GDF9* showed reduced mRNAs (between 60

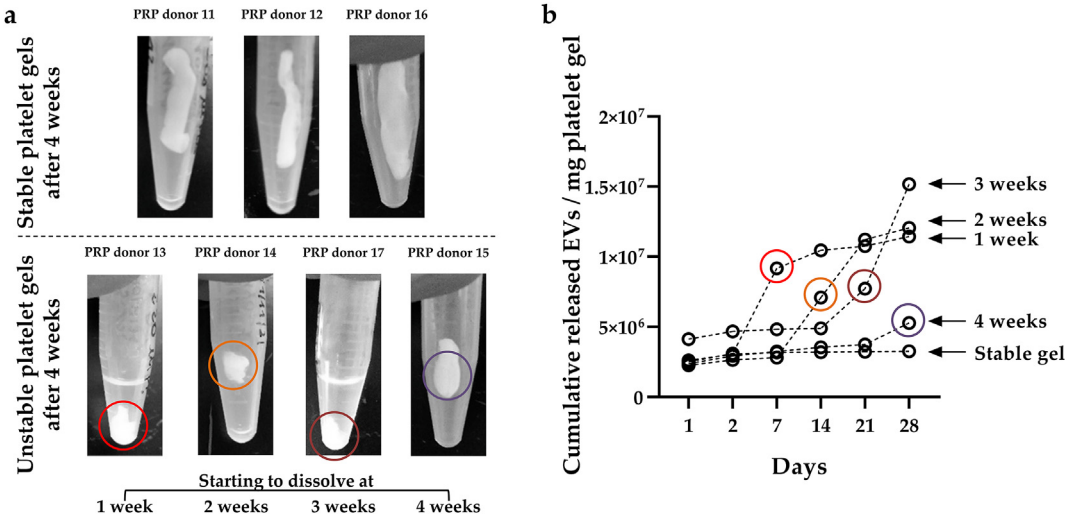

Fig. 7. Unstable platelet gels increase EVs release with dissolution. a) At 4 weeks after clot formation, stable platelet gels have intact structure and shape while unstable clots reduced size with those started to dissolve between 1 and 3 week having smaller dimension. Representative pictures are shown. b) The cumulative EVs release for representative unstable gels (one per starting week of dissolution) with respect to the mean of stable clots is shown.

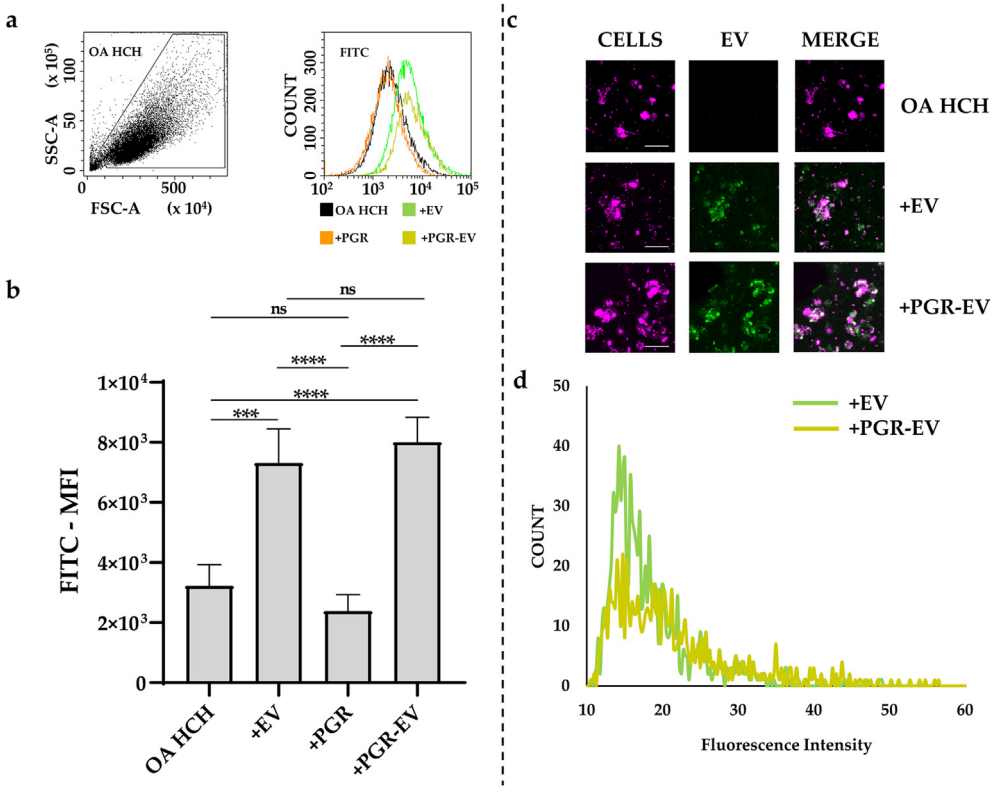

Fig. 8. EVs uptake in OA patients' chondrocytes. a) Flow cytometry of OA patients' chondrocytes (OA HCH) treated with purified EVs (EV), platelet gel released (PGR) and platelet gel + EVs released (PGR-EV). Plots of a representative OA HCH donor are shown. b) Mean fluorescence intensity (MFI) of the FITC channel detecting signal of fluorescent EVs is reported for the four different treatments. No statistical significant (p-value <0.05) difference between purified EVs and EVs in the platelet gel released was detected. Mean ± SEM, n = 3, ns for not significant, *** for p-value <0.001 and **** for p-value <0.0001. c) Pictures after 48 h of OA chondrocytes grown in 3D chips and incubated with EVs, either purified or released from platelet gel. EVs were CFSE-stained and are shown in green, whereas cells were stained with CellTracker™ Deep Red Dye and are shown in violet. The merged pictures clearly show the overlapping of the signal of ASC-EVs with cells. One representative donor is shown. Scale bar for 50 μm. d) Green fluorescence intensity of OA chondrocytes inside the 3D microfluidic devices, incubated for 48 h with pure EVs or EVs in the platelet gel released. Reported intensity plots are the mean of fluorescent signal for three independent donors. Similar amounts of EVs were added. For fluorescent signals, only intensities above the background of untreated chondrocytes (arbitrary value of 10) are shown.

and 98 %). As for EVs, *MMP1* and *MMP3* reduced their expression at around 50 % of their levels. Of note, released of gels with EVs had the strongest effect on chondrocytes since all genes downregulated by either single EVs or platelet gel resulted even more significantly reduced, while those genes upregulated by platelet gel released had a contraction of their upregulation, reducing the possible pro-inflammatory effects. This was clearly shown by the direct comparison of gel released without and with EVs, where all analysed factors had a stronger downregulation in presence of EVs (Fig. 10b). In particular, many factors resulted downregulated of a factor >50

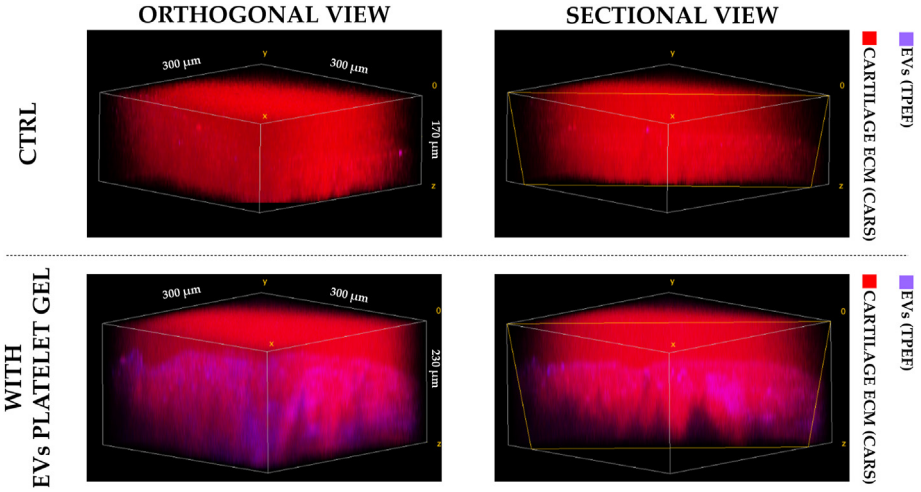

Fig. 9. 3D reconstructions of the cartilage after incubation with platelet gels without and with EVs. CARS signal in red originating mainly by cartilage ECM and TPEF signal related to the EVs fluorescence shown in blue. Close to the boundary box the dimensions in μm are shown starting from the origin vertex.

GENE	a) vs OA chondrocytes +EV	+PGR	+PGR-EV	b) vs +PGR +PGR-EV	c) Combinatorial PGR/EV effect 1 = additive <1 synergistic	ROLE OF THE GENE/PROTEIN IN CARTILAGE DAMAGE
IL1B	*0.79*	24.77	12.75	**0.41**	0.65	Upregulates the major extracellular proteolytic enzymes in cartilage degradation
IL6	**0.73**	**0.32**	**0.24**	**0.73**	1.03	Potentiates the catabolic effects of IL-1β and serves as catabolic mediator
IL8	**0.71**	*1.62*	**0.54**	**0.37**	0.47	Favors the direct invasion of cartilage by synoviocytes and macrophages that erode and degrade cartilage
IL11	**1.15**	**12.85**	**8.84**	**0.67**	0.60	Stimulates cartilage damage by inducing aggrecanase activity
CCL5	**0.74**	**0.22**	**0.13**	**0.53**	0.78	Upregulates metalloproteases expression
CCL8	**0.82**	**0.02**	**0.01**	**0.60**	0.75	Pro-inflammatory cytokine upregulated in OA cartilage
TNFSF11	**0.74**	**0.38**	**0.10**	**0.28**	0.37	Induces chondrocyte apoptosis and matrix loss by degrading matrix metalloproteinases
FGF2	1.18	**2.15**	1.57	**0.70**	0.62	Triggers proteoglycan depletion in cartilage and upregulates metalloproteinases expression
GDF9	**0.66**	**0.35**	**0.21**	**0.64**	0.93	Affects subchondral bone density, including both cortical and trabecular bone mineral density
IDO1	0.94	1.05	0.55	**0.31**	0.56	Impairs chondrogenic differentiation of progenitor cells
COX2	**0.61**	0.97	*0.49*	**0.43**	0.83	Increases cartilage proteoglycan degradation
CTSS	0.97	0.64	**0.45**	**0.63**	0.73	Displays aggrecanase activity
MMP1	**0.43**	**0.45**	**0.13**	**0.28**	0.68	Degrades the extracellular matrix subsequently damaging cartilage and altering biomechanical properties
MMP3	**0.72**	**0.59**	**0.28**	**0.49**	0.66	Degrades the extracellular matrix subsequently damaging cartilage and altering biomechanical properties

Fig. 10. EVs, platelet gel released and combination effect on OA chondrocytes transcriptional profile. a) OA-related gene up- or down-regulation in OA chondrocytes exposed to EVs, 48 h' platelet gel released (PGR) and 48 h' platelet gel + EVs released (PGR-EV). b) The presence of EVs empowered the protective effect of PGR and reduced the increase of pro-inflammatory mediators. c) The PGR-EV effect (fold change) was superior to the expected sum of the PGR and EV single effects calculated under the formula EV fold change * PGR fold change. When the ratio (obtained/expected) was <1 a synergistic effect was present. Fold change mean values are shown (n = 5). For column a and b, italics is for p-value <0.1 and bold for p-value <0.05.

%, with the most OA relevant protein-coding genes *IL1β/8* and *MMP1/3* falling in this group. Eventually, to understand whether the combined effect of platelet gel released and EVs was additive or synergistic, we compared the results of the combination with those expected considering a sum of the single outcomes as per the formula = EVs fold change * platelet gel released fold change (Fig. 10c). Notably, except for *IL6*, the gene expression reduction of the combination was lower than predicted, with an average for all genes of 0.69 ± 0.17 (p-value <0.0001 with respect to hypothesis set as 1), suggesting that the two products together have a synergistic effect possibly stimulating separate pathways.

Eventually, EVs and platelet gel released without or with EVs were able to promote chondrocytes growth with respect to untreated samples (fold for EVs 1.40 ± 0.23, p-value 0.0093; platelet gel released 1.81 ± 0.18, p-value 0.0116; platelet gel with EVs released 1.94 ± 0.22, p-value 0.0120; n = 5). For this parameter, the combination of EVs and platelet gel released did not result in a significant increase of cell proliferation with respect to gel released alone (ratio of 1.075 ± 0.05, p-value 0.2250; n = 5).

4. Discussion

In this manuscript, we described a new methodology to incorporate adipose ASC-EVs into platelet gels with high efficiency.

One of the crucial points for the proposed protocol, in view of clinical translation, is the amount of EVs to be supplemented to produce the platelet gel. The EVs number to be added to 1 ml of PRP for gel formation used in this study (1×10^{10}), was derived by investigating literature data. A large multicentre trial based on ASCs intra-articular administration to knee OA patients described the use of 10^7 cells as the most effective condition [31], further supported by other trials where similar (10^7 range) number of ASCs was administered to patients [32–34] with cartilage defects, when disclosed, up to 4 cm^2. Our data showed that around 5000 EVs may be released in 48 h per ASC, thus for 10^7 cells around 5×10^{10} particles may be dispersed in the joint. This number is similar to the amount of EVs claimed to be administered in the NCT05060107 [23] and NCT05261360 [24] clinical trials (10×10^{10} range). Moreover, articular surface and bone cartilage interface in the knee was evaluated with magnetic resonance imaging techniques to be around 100 cm^2 [35]. Taking into account the usual size of cartilage lesions treated with microfractures or ASCs in trials (for ease of calculation considered 2 cm^2), this would mean that around 1/50 of EVs could be available to the lesion area (approximately 1–2 x 10^9). This value is largely rounded up to the highest value, since in the articular joints other surfaces other than cartilage are present and ASC-released EVs are dispersed in the synovial fluid being therefore physically distant from cartilage surface. In our protocol, 1×10^{10} EVs are added to 1 ml PRP with an average 60 % incorporation into platelet gels, meaning roughly 5×10^9 particles per clot. Being each clot we produced in 1.5 ml tubes of a size around 1 × 0.4 cm (area of 0.4 cm^2), we calculated 5 × 1 ml gels or 1 gel obtained from 5 ml PRP to fill a 2 cm^2 defect (taken as representative size for small to medium lesions) for an amount of incorporated EVs of 2.5×10^{10} out of 5×10^{10} input particles, a value at least 50% lower than to the one used in the clinical trials. This value of incorporated particles in direct contact with cartilage is under the most conservatives estimates 10–25 times higher than what postulated for EVs secreted directly by ASCs or administered in the clinical trials. Being EVs released in 48 h 7 % of incorporated, and considering that only half of clot surface is in contact with the lesion, approximately 1×10^9 EVs may directly be transferred from platelet gel to the lesion, as we demonstrated with fluorescent EVs incorporation into *ex vivo* cartilage fragments from OA patients. Another 1×10^9 EVs quote is released from the other side of the clot, being anyway very close to cartilage with respect to the same

amount of EVs produced by cells and dispersed in the synovial fluid. Moreover, EVs are constantly released up to 4 weeks, although at a lower ratio with respect to initial 48 h. In this perspective, unstable PRP gels might give a view of what may happen in patients' joints. In fact, if *in vitro* more than half of clots remained solid, in animal models it has been estimated that platelet gels get completely dissolved between 1 and 3 weeks [14]. The strong increase of EVs exit concomitant to gel dissolution herein reported suggests that a larger release of EVs directly at site of lesion will occur during a time lapse of 1–3 weeks after gel placement.

ASC-EVs used in this study showed a large number of factors, both miRNAs and proteins, involved in cartilage protection and inflammation modulation. This is in agreement with previous reports of our group for EVs obtained from ASCs cultivated in different media [36] or isolated from alternative sources [37]. Among miRNA targets, several genes coding for the most characterized and OA-related cytokines such as *IL1B*, *IL6*, *IL8*, *TNFA* and *IFNG* appeared. Inflammatory mediators are both primary and secondary regulators of cartilage damage, and their management is crucial for tissue recovery [38] and proper healing alongside a tight regulation of extracellular matrix degrading enzymes [39]. In this frame EV-miRNAs also may interact with a number of genes coding for MMPs and other metalloproteases, that are directly responsible for cartilage loss and weaker structure and are upregulated in fibrochondrocytes [40]. Consistently, growth factors reported to contribute to cartilage degradation or inflammation are targeted as well. As an example, VEGF is associated with catabolic processes in chondrocytes and its increased expression correlates with increased disease severity [41], similarly to TGF-β1/2 and CTGF whose balance must be tightly regulated. In fact, under OA or cartilage damage, an abnormal increase (CTGF) [42] or bioavailability (TGF-β1/2) [43] occur with increase in inflammation and matrix degenerescence. For instance, if naïve TGF-β may stimulate ECM production [44], it is also able to prompt osteophytes similar to those found in OA [45]. Also, in the frame of a tight balance of their amounts, CTGF and TGF-β1 may induce fibrotic proteins including Col I/III, and α–SMA while downregulating healthy cartilage development–associated proteins including Sox9 and Col II [46]. Moreover, VEGFA is involved in pain [47], as well as other two miRNA-targets BDNF [48] and NGF [49], suggesting that EVs activity goes beyond tissue restoration and inflammation management. Of note, these results were corroborated analysing the reported role of EV-miRNAs at tissue and cell type levels, where a 3 to 4-fold higher amount for anti-inflammatory and cartilage protective players was detected, respectively. In this perspective, the miRNA with a wider effect was miR-24-3p reported to attenuate chondrocyte injury [50] and cartilage degradation [50], as well as inhibit Mφ activation and pro-inflammatory cytokine production [51]. Supporting this notion of EVs able to modulate cartilage and inflammation, not only miRNAs but also factors associated with EVs had similar properties. In fact, several proteins identified with ELISA have a direct involvement with extracellular matrix organization, as highlighted by connective tissue and cartilage development related factors, and immune cells. Among the last ones, chemotaxis hold the way. This is in agreement with the proposed role of MSCs that, through secreted factors and EVs, are able to attract and interact with immune cells to downgrade their inflammatory phenotype [52]. As a whole, miRNAs and proteins suggest the ability of EVs in favouring cartilage homeostasis both directly acting on ECM enzymes and indirectly modulating the inflammatory environment that surrounds damaged and healing tissue.

Molecular data were supported by the *in vitro* experiments on OA patients' chondrocytes. EVs had an anti-inflammatory and ECM protective activity, the basis to foster tissue stability and integrity and confirming what proposed in several *in vitro* and *in vivo* models [53]. A similar result was obtained for cells cultured in presence of platelet gel released, with the increase in *IL1β* and *IL11* after 48 h supporting the concept that platelet products have a direct beneficial effect on articular chondrocytes by driving in sequence a transient activation and the resolution of the inflammatory process [54]. Of note, the combination of EVs and factors released by platelet gels had a synergic effect, maintaining even if at lower rate the beneficial inflammatory step given by the platelet products and enhancing the reduction of the other factors involved in cartilage damage and degradation. This result suggests that EVs and gel released molecules may act on separate pathways and their concomitant activation may multiply rather than sum the different responses. In this view, several of tested genes were reported as target of EV-miRNAs. Moreover, both EVs and platelet gel released factors were able to enhance chondrocyte proliferation although at different rates, with plasma factors being more potent inducers. For this parameter, the combination did not lead to enhanced growth, suggesting that the strong proliferative effect of platelet molecules overcome those of EVs. This is in agreement with the postulated use of PRP and platelet products as human supplement to enhance cell growth in place of FBS [55]. To corroborate these preliminary data *in vitro*, further *ex vivo* and *in vivo* experiments will be needed to assess the efficacy of released EVs and factors on cartilage strength over time.

This work has some limitations. For sake of simplicity and ease of translatability to everyday clinical practice we opted to prepare the PRP fibrin gel with a commercial kit. The simplicity of the protocol herein described will easily allow to apply the procedure to other methods based on a similar principle. Further, a pool of EVs was used due to the high similarity among donors. For future studies, the concept of the pool of different samples or the idea of a "superdonor" or modified EVs with improved properties may be explored. In this frame, the gender impact on EVs performance should also be addressed, being the present study obtained with female donors only to reduce ASCs' variability. Eventually, the use of pathologic chondrocytes allowed for a first demonstration of EV-loaded PRP-gel superior and synergic activity, with the limitations given by *in vitro* models. The future step of this project will be to confirm these results in *in vivo* models before testing in clinical studies, with focus on gel stability differences between patients that could affect EVs release over time.

5. Conclusions

This research describes the rationale for a high efficiency protocol for embedding MSC-EVs in platelet-derived fibrin gels following an easy modification of the procedure routinely used in surgery rooms. Thus, alongside its relevance on the manufacturing point of view, the described biological product will be an interesting option in the wake of procedures familiar to orthopaedic surgeons that will not require specific training helping in translating this technology to everyday clinical practice. The favourable results *in vitro* on pathologic chondrocytes will lay the foundations for future research in pre-clinical models, a crucial step to eventually bring EV-gels to patients as a new string to the bows of orthopaedic surgeons aiming at stop or delay the need of prosthetic implants for focal lesions, especially in young subjects not ready for metal.

Ethics approval and consent to participate

The study was conducted in accordance with the Declaration of Helsinki, and approved by San Raffaele Hospital Ethics Committee ("Caratterizzazione e valutazione del potenziale rigenerativo delle

cellule progenitrici tessuto specifiche ottenute da tessuto muscoloscheletrici", approval on date 16 December 2020, registered under number 214/int/2020 for surgery room waste material; "Utilizzo dei Patient-Reported Outcome Measures (PROMs), delle valutazioni cliniche oggettive e biomolecolari per il monitoraggio dei pazienti sottoposti a trattamenti di medicina rigenerativa presso il Centro REGAIN-Regenerative Galeazzi Institute", approval on date 8 March 2018, registered under number 6/int/2018 for regenerative medicine procedures waste material). Informed consent was obtained from all subjects involved in the study.

Funding

The work reported in this publication was funded by the Italian Ministry of Health, "Ricerca Corrente". The APC was funded by the Italian Ministry of Health, "Ricerca Corrente". Funder has not a specific role in the conceptualization, design, data collection, analysis, decision to publish, or preparation of the manuscript.

CRediT authorship contribution statement

Conceptualization, ER, PDL and LdG; methodology, ER and PDL; software, SL and GT; validation, ER and PDL; formal analysis, ER, PDL, SP and LM.; investigation, ER and PDL; resources, FV; data curation, GT; writing—original draft preparation, ER; writing—review and editing, LdG and MM; visualization, GT; supervision, LdG; project administration, ER; funding acquisition, ER and LdG. All authors have read and agreed to the published version of the manuscript.

Consent for publication

Not applicable. No participating patients may be identified.

Data availability

The datasets generated and/or analysed during the current study are available in the OSF repository, https://osf.io/3jaq7/?view_only=eb1f7fefdaae4c509af4b24c04857696.

Declaration of competing interest

The authors declare that they have no known competing financial interests or personal relationships that could have appeared to influence the work reported in this paper. All authors guarantee the originality of the study and ensure that it has not been published previously. All the listed authors have read and approved the submitted manuscript.

Acknowledgments

Authors wish to thank all collaborators of the RE.GA.IN.® Center of IRCCS Ospedale Galeazzi – Sant'Ambrogio for their help and support. Authors want to acknowledge Università degli Studi di Milano for supporting and promoting this project under the "Seed4Innovation" program.

Appendix A. Supplementary data

Supplementary data to this article can be found online at https://doi.org/10.1016/j.reth.2024.06.020.

References

[1] Lories RJ, Luyten FP. The bone-cartilage unit in osteoarthritis. Nat Rev Rheumatol 2011. https://doi.org/10.1038/nrrheum.2010.197.
[2] Matsushita T, Tokura T, Okimura K, Sano S, Nishida K, Nagai K, et al. Surgical treatment of cartilage lesions in the knee: a narrative review. J Joint Surg Res 2023. https://doi.org/10.1016/j.jjoisr.2023.02.001.
[3] Widuchowski W, Lukasik P, Kwiatkowski G, Faltus R, Szyluk K, Widuchowski J, et al. Isolated full thickness chondral injuries. Prevalance and outcome of treatment. A retrospective study of 5233 knee arthroscopies. Acta Chir Orthop Traumatol Cech 2008;75:382–6.
[4] Flanigan DC, Harris JD, Trinh TQ, Siston RA, Brophy RH. Prevalence of chondral defects in athletes' knees: a systematic review. Med Sci Sports Exerc 2010. https://doi.org/10.1249/MSS.0b013e3181d9eea0.
[5] Lim WB, Al-Dadah O. Conservative treatment of knee osteoarthritis: a review of the literature. World J Orthoped 2022. https://doi.org/10.5312/wjo.v13.i3.212.
[6] Xie X, Zhang C, Tuan RS. Biology of platelet-rich plasma and its clinical application in cartilage repair. Arthritis Res Ther 2014. https://doi.org/10.1186/ar4493.
[7] Solanki K, Shanmugasundaram S, Shetty N, Kim SJ. Articular cartilage repair & joint preservation: a review of the current status of biological approach. J Clin Orthop Trauma 2021. https://doi.org/10.1016/j.jcot.2021.101602.
[8] Medina J, Garcia-Mansilla I, Fabricant PD, Kremen TJ, Sherman SL, Jones K. Microfracture for the treatment of symptomatic cartilage lesions of the knee: a survey of international cartilage regeneration & joint preservation society. Cartilage 2021. https://doi.org/10.1177/1947603520954503.
[9] Case JM, Scopp JM. Treatment of articular cartilage defects of the knee with microfracture and enhanced microfracture techniques. Sports Med Arthrosc Rev 2016. https://doi.org/10.1097/JSA.0000000000000113.
[10] Gu Y, Wang G, Chen P. Platelet rich plasma combined with arthroscopic microfracture versus arthroscopic microfracture alone for the treatment of knee cartilage injury. Am J Transl Res 2023;15:3705–13.
[11] Papalia R, Diaz Balzani L, Torre G, Tirindelli MC, Nobile C, Maffulli N, et al. Intraoperative application Platelet rich fibrin, postoperative injections OF PRP or microfracture only for osteochondral lesions of the knee: a five-year retrospective evaluation. J Biol Regul Homeost Agents 2016;30:41–9.
[12] Zumstein MA, Berger S, Schober M, Boileau P, Nyffeler RW, Horn M, et al. Leukocyte- and platelet-rich fibrin (L-PRF) for long-term delivery of growth factor in rotator cuff repair: review, preliminary results and future directions. Curr Pharmaceut Biotechnol 2012. https://doi.org/10.2174/138920112800624337.
[13] Nakanishi Y, Matsushita T, Nagai K, Araki D, Hoshino Y, Kuroda R. Fibrin clot and Leukocyte-rich platelet-rich fibrin show similar release kinetics and amount of growth factors: a pilot study. J Orthop Surg Res 2023. https://doi.org/10.1186/s13018-023-03709-5.
[14] Yamashita Y, Chen K, Kuroda S, Kasugai S. Stability of platelet-rich fibrin in vivo: histological study in rats. J Oral Tissue Eng 2016. https://doi.org/10.11223/jarde.14.83.
[15] Ragni E, Perucca Orfei C, Valli F, Zagra L, de Girolamo L. Molecular characterization of secreted factors and extracellular vesicles-embedded miRNAs from bone marrow-derived mesenchymal stromal cells in presence of synovial fluid from osteoarthritis patients. Biology 2022. https://doi.org/10.3390/biology11111632.
[16] Ragni E, Papait A, Perucca Orfei C, Silini AR, Colombini A, Viganò M, et al. Amniotic membrane-mesenchymal stromal cells secreted factors and extracellular vesicle-miRNAs: anti-inflammatory and regenerative features for musculoskeletal tissues. Stem Cells Transl Med 2021. https://doi.org/10.1002/sctm.20-0390.
[17] Ragni E, Perucca Orfei C, De Luca P, Colombini A, Viganò M, de Girolamo L. Secreted factors and EV-miRNAs orchestrate the healing capacity of adipose mesenchymal stem cells for the treatment of knee osteoarthritis. Int J Mol Sci 2020. https://doi.org/10.3390/ijms21051582.
[18] Mortati L, de Girolamo L, Perucca Orfei C, Viganò M, Brayda-Bruno M, Ragni E, et al. In vitro study of extracellular vesicles migration in cartilage-derived osteoarthritis samples using real-time quantitative multimodal nonlinear optics imaging. Pharmaceutics 2020. https://doi.org/10.3390/pharmaceutics12080734.
[19] Ragni E, Palombella S, Lopa S, Talò G, Perucca Orfei C, De Luca P, et al. Innovative visualization and quantification of extracellular vesicles interaction with and incorporation in target cells in 3D microenvironments. Cells 2020. https://doi.org/10.3390/cells9051180.
[20] Cosenza S, Ruiz M, Toupet K, Jorgensen C, Noël D. Mesenchymal stem cells derived exosomes and microparticles protect cartilage and bone from degradation in osteoarthritis. Sci Rep 2017. https://doi.org/10.1038/s41598-017-15376-8.
[21] To K, Romain K, Mak C, Kamaraj A, Henson F, Khan W. The treatment of cartilage damage using human mesenchymal stem cell-derived extracellular vesicles: a systematic review of in vivo studies. Front Bioeng Biotechnol 2020. https://doi.org/10.3389/fbioe.2020.00580.
[22] Kim YG, Choi J, Kim K. Mesenchymal stem cell-derived exosomes for effective cartilage tissue repair and treatment of osteoarthritis. Biotechnol J 2020. https://doi.org/10.1002/biot.202000082.

[23] ClinicalTrails.gov. https://clinicaltrials.gov/study/NCT05060107. Accessed 5 April 2024.
[24] ClinicalTrials.gov. https://clinicaltrials.gov/study/NCT05261360. Accessed 5 April 2024.
[25] Szklarczyk D, Gable AL, Lyon D, Junge A, Wyder S, Huerta-Cepas J, et al. STRING v11: protein-protein association networks with increased coverage, supporting functional discovery in genome-wide experimental datasets. Nucleic Acids Res 2019. https://doi.org/10.1093/nar/gky1131.
[26] Pergoli L, Cantone L, Favero C, Angelici L, Iodice S, Pinatel E, et al. Extracellular vesicle-packaged miRNA release after short-term exposure to particulate matter is associated with increased coagulation. Part Fibre Toxicol 2017. https://doi.org/10.1186/s12989-017-0214-4.
[27] Huang HY, Lin YC, Cui S, Huang Y, Tang Y, Xu J, et al. miRTarBase update 2022: an informative resource for experimentally validated miRNA-target interactions. Nucleic Acids Res 2022. https://doi.org/10.1093/nar/gkab1079.
[28] Chou CH, Jain V, Gibson J, Attarian DE, Haraden CA, Yohn CB, et al. Synovial cell cross-talk with cartilage plays a major role in the pathogenesis of osteoarthritis. Sci Rep 2020. https://doi.org/10.1038/s41598-020-67730-y.
[29] Endisha H, Rockel J, Jurisica I, Kapoor M. The complex landscape of microRNAs in articular cartilage: biology, pathology, and therapeutic targets. JCI Insight 2018. https://doi.org/10.1172/jci.insight.121630.
[30] Xu SJ, Hu HT, Li HL, Chang S. The role of miRNAs in immune cell development, immune cell activation, and tumor immunity: with a focus on macrophages and natural killer cells. Cells 2019. https://doi.org/10.3390/cells8101140.
[31] CORDIS. https://cordis.europa.eu/project/id/241719. Accessed on 5 April 2024.
[32] Freitag J, Bates D, Wickham J, Shah K, Huguenin L, Tenen A, et al. Adipose-derived mesenchymal stem cell therapy in the treatment of knee osteoarthritis: a randomized controlled trial. Regen Med 2019. https://doi.org/10.2217/rme-2018-0161.
[33] Lu L, Dai C, Zhang Z, Du H, Li S, Ye P, et al. Treatment of knee osteoarthritis with intra-articular injection of autologous adipose-derived mesenchymal progenitor cells: a prospective, randomized, double-blind, active-controlled, phase IIb clinical trial. Stem Cell Res Ther 2019. https://doi.org/10.1186/s13287-019-1248-3.
[34] Koh YG, Kwon OR, Kim YS, Choi YJ, Tak DH. Adipose-derived mesenchymal stem cells with microfracture versus microfracture alone: 2-year follow-up of a prospective randomized trial. Arthroscopy 2016. https://doi.org/10.1016/j.arthro.2015.09.010.
[35] Hohe J, Ateshian G, Reiser M, Englmeier KH, Eckstein F. Surface size, curvature analysis, and assessment of knee joint incongruity with MRI in vivo. Magn Reson Med 2002. https://doi.org/10.1002/mrm.10097.
[36] Ragni E, Perucca Orfei C, De Luca P, Mondadori C, Viganò M, Colombini A, et al. Inflammatory priming enhances mesenchymal stromal cell secretome potential as a clinical product for regenerative medicine approaches through secreted factors and EV-miRNAs: the example of joint disease. Stem Cell Res Ther 2020. https://doi.org/10.1186/s13287-020-01677-9.
[37] Colombini A, Libonati F, Lopa S, Ragni E, De Luca P, Zagra L, et al. Immunomodulatory potential of secretome from cartilage cells and mesenchymal stromal cells in an arthritic context: from predictive fiction toward reality. Front Med 2022. https://doi.org/10.3389/fmed.2022.992386.
[38] Goldring MB, Otero M. Inflammation in osteoarthritis. Curr Opin Rheumatol 2011. https://doi.org/10.1097/BOR.0b013e328349c2b1.
[39] Yamamoto K, Wilkinson D, Bou-Gharios G. Targeting dysregulation of metalloproteinase activity in osteoarthritis. Calcif Tissue Int 2021. https://doi.org/10.1007/s00223-020-00739-7.
[40] Deschner J, Rath-Deschner B, Agarwal S. Regulation of matrix metalloproteinase expression by dynamic tensile strain in rat fibrochondrocytes. Osteoarthritis Cartilage 2006. https://doi.org/10.1016/j.joca.2005.09.005.
[41] Nagao M, Hamilton JL, Kc R, Berendsen AD, Duan X, Cheong CW, et al. Vascular endothelial growth factor in cartilage development and osteoarthritis. Sci Rep 2017. https://doi.org/10.1038/s41598-017-13417-w.
[42] Yang Z, Li W, Song C, Leng H. CTGF as a multifunctional molecule for cartilage and a potential drug for osteoarthritis. Front Endocrinol 2022. https://doi.org/10.3389/fendo.2022.1040526.
[43] van der Kraan PM. Differential role of transforming growth factor-beta in an osteoarthritic or a healthy joint. J Bone Metab 2018. https://doi.org/10.11005/jbm.2018.25.2.65.
[44] Pelletier JP, Roughley PJ, DiBattista JA, McCollum R, Martel-Pelletier J. Are cytokines involved in osteoarthritic pathophysiology? Semin Arthritis Rheum 1991. https://doi.org/10.1016/0049-0172(91)90024-t.
[45] van Beuningen HM, van der Kraan PM, Arntz OJ, van den Berg WB. Transforming growth factor-beta 1 stimulates articular chondrocyte proteoglycan synthesis and induces osteophyte formation in the murine knee joint. Lab Invest 1994;71:279–90.
[46] Li J, Jiang H, Lv Z, Sun Z, Cheng C, Tan G, et al. Articular fibrocartilage-targeted therapy by microtubule stabilization. Sci Adv 2022. https://doi.org/10.1126/sciadv.abn8420.
[47] Ma K, Singh G, Wang J, O-Sullivan I, Votta-Velis G, Bruce B, et al. Targeting vascular endothelial growth factor receptors as a therapeutic strategy for osteoarthritis and associated pain. Int J Biol Sci 2023. https://doi.org/10.7150/ijbs.79125.
[48] Gowler PRW, Li L, Woodhams SG, Bennett AJ, Suzuki R, Walsh DA, et al. Peripheral brain-derived neurotrophic factor contributes to chronic osteoarthritis joint pain. Pain 2020. https://doi.org/10.1097/j.pain.0000000000001694.
[49] Miller RE, Block JA, Malfait AM. Nerve growth factor blockade for the management of osteoarthritis pain: what can we learn from clinical trials and preclinical models? Curr Opin Rheumatol 2017. https://doi.org/10.1097/BOR.0000000000000354.
[50] Xu J, Qian X, Ding R. MiR-24-3p attenuates IL-1β-induced chondrocyte injury associated with osteoarthritis by targeting BCL2L12. J Orthop Surg Res 2021. https://doi.org/10.1186/s13018-021-02378-6.
[51] Fordham JB, Naqvi AR, Nares S. miR-24 regulates macrophage polarization and plasticity. J Clin Cell Immunol 2015. https://doi.org/10.4172/2155-9899.1000362.
[52] Planat-Benard V, Varin A, Casteilla L. MSCs and inflammatory cells crosstalk in regenerative medicine: concerted actions for optimized resolution driven by energy metabolism. Front Immunol 2021. https://doi.org/10.3389/fimmu.2021.626755.
[53] Ng CY, Chai JY, Foo JB, Mohamad Yahaya NH, Yang Y, Ng MH, et al. Potential of exosomes as cell-free therapy in articular cartilage regeneration: a review. Int J Nanomed 2021. https://doi.org/10.2147/IJN.S327059.
[54] Pereira RC, Scaranari M, Benelli R, Strada P, Reis RL, Cancedda R, et al. Dual effect of platelet lysate on human articular cartilage: a maintenance of chondrogenic potential and a transient proinflammatory activity followed by an inflammation resolution. Tissue Eng 2013. https://doi.org/10.1089/ten.TEA.2012.0225.
[55] Mohamed HE, Asker ME, Kotb NS, El Habab AM. Human platelet lysate efficiency, stability, and optimal heparin concentration required in culture of mammalian cells. Blood Res 2020. https://doi.org/10.5045/br.2020.55.1.35.